RADC-TR-81-353
Final Technical Report
December 1981

AD A113174

ATTENUATION AND SCATTERING OF LIGHT IN OPTICAL FIBERS-EFFECTS OF NUCLEAR RADIATION (MODULATION & DISPLAY OF LASER RADIATION)

Department of Electrical Engineering
UNIV of RHODE ISLAND

Shashanka S. Mitra

APPROVED FOR PUBLIC RELEASE; DISTRIBUTION UNLIMITED

DTIC
SELECTE
APR 8 1982
H

ROME AIR DEVELOPMENT CENTER
Air Force Systems Command
Griffics Air Force Base, New York 13441

82 04 08 044

This report has been reviewed by the RADC Public Affairs Office (PA) and is releasable to the National Technical Information Service (NTIS). At NTIS it will be releasable to the general public, including foreign nations.

RADC-TR-83-253 has been reviewed and is approved for publication.

APPROVED: *James A. Wall*

JAMES A. WALL
Project Engineer

APPROVED: *James F. Hines*

JAMES F. HINES, Major, USAF
Deputy Director
Solid State Sciences Division

FOR THE COMMANDER: *John P. Huss*

JOHN P. HUSS
Acting Chief, Plans Office

If your address has changed or if you wish to be removed from the RADC mailing list, or if the addressee is no longer employed by your organization, please notify RADC (ESR) Hanscom AFB MA 01731. This will assist us in maintaining a current mailing list.

Do not return copies of this report unless contractual obligations or notices on a specific document requires that it be returned.

RADC-TR-81-353

Title: ATTENUATION AND SCATTERING OF LIGHT IN OPTICAL FIBERS-EFFECT
        OF NUCLEAR RADIATION (MODULATION & DISPLAY OF LASER RADIATION)

Dated: December 1981

Please add the following to cover: University of Rhode Island

UNCLASSIFIED

REPORT DOCUMENTATION PAGE		READ INSTRUCTIONS BEFORE COMPLETING FORM
1. REPORT NUMBER RADC-TR-81-353	2. GOVT ACCESSION NO. AP-A113174	3. RECIPIENT'S CATALOG NUMBER
4. TITLE (and Subtitle) ATTENUATION AND SCATTERING OF LIGHT IN OPTICAL FIBERS-EFFECTS OF NUCLEAR RADIATION (MODULATION & DISPLAY OF LASER RADIATION)		5. TYPE OF REPORT & PERIOD COVERED Final Technical Report 1 May 77 - 30 Apr 80
		6. PERFORMING ORG. REPORT NUMBER N/A
7. AUTHOR(s) Shashanka S. Mitra		8. CONTRACT OR GRANT NUMBER(s) F19628-77-C-0109
9. PERFORMING ORGANIZATION NAME AND ADDRESS Department of Electrical Engineering University of Rhode Island Kingston RI 02881		10. PROGRAM ELEMENT, PROJECT, TASK AREA & WORK UNIT NUMBERS 61102F 2306J322
11. CONTROLLING OFFICE NAME AND ADDRESS Deputy for Electronic Technology (RADC/ESR) Hanscom AFB MA 01731		12. REPORT DATE December 1981
		13. NUMBER OF PAGES 98
14. MONITORING AGENCY NAME & ADDRESS(if different from Controlling Office) Same		15. SECURITY CLASS. (of this report) UNCLASSIFIED
		15a. DECLASSIFICATION/DOWNGRADING SCHEDULE N/A

16. DISTRIBUTION STATEMENT (of this Report)

Approved for public release; distribution unlimited.

17. DISTRIBUTION STATEMENT (of the abstract entered in Block 20, if different from Report)

Same

18. SUPPLEMENTARY NOTES

RADC Project Engineer: James A. Wall (ESR)

19. KEY WORDS (Continue on reverse side if necessary and identify by block number)

Optical Fibers	Pulse Shape
Light Attenuation	Pulse Broadening
Light Scattering	Nuclear Radiation Effects

20. ABSTRACT (Continue on reverse side if necessary and identify by block number)

This study consists of measurements of effects of nuclear radiation on attenuation and pulse dispersion and light scattering in optical fibers. The radiation induced attenuation in a numer of optical fibers has been evaluated. Several different types of fibers were exposed to steady state nuclear radiation and the resulting decrease in transmitted power was monitored as a function of wavelength and radiation dose. The wavelengths examined were in the visible and near IR regions that are of

DD FORM 1 JAN 73 1473 EDITION OF 1 NOV 65 IS OBSOLETE

UNCLASSIFIED

specific interest for optical fiber communications. The fibers showed a decrease in transmitted power at all wavelengths examined. The radiation sensitivity in glass core fibers was observed to show dependence on factors such as impurity content and the index modifying dopants in the fiber.

Experimental measurements of neutron radiation induced pulse dispersion changes, and attenuation changes in a 100 μm core step index fiber were made. In the course of irradiation pulse dispersion in the fiber was observed to decrease while the attenuation increased. The results indicate greater decreases in the transmission of higher order modes. This reflects the fact that the radiation response of a fiber is determined by the respective refractive indices and absorption coefficients of both the core and cladding of the fiber. Results are presented along with a discussion of mechanisms by which dispersion changes can occur in irradiated fibers.

The light scattering spectra of optical fibers were reviewed. The results include Raman spectra of fused silica fibers and effects of dopants and irradiation. Large scattering volumes available in optical fibers afford one to detect low dopant concentrations and relatively weak second order spectra. Low frequency Raman spectra of optical fibers show the expected non-Debye type anomaly.

PREFACE

This final report describes the research performed under Contract No. F 19628-77-C-0109 from 1 May, 1977 to 30 April, 1980. The primary research objective of this project was experimental measurement of effect of neutron irradiation on attenuation and pulse broadening and light scattering in optical fibers. In carrying out this research the principal investigator was assisted by the following: Dr. P.K. Banerjee, Mr. A.J. Corey, Mr. J. Jacobs, Mr. G. Lan, and Mr. R. Rao. In addition to four papers, one dissertation, accepted for the award of an M.S. degree by the University of Rhode Island, resulted from this research. The published papers are:

1. "Optical Absorption Spectra of Neutron Irradiated Optical Fibers in the 0.7 to 1.1 μm Region" by R. Rao, A.J. Corey, and S.S. Mitra in Fiber Optics, eds. B. Bendow and S.S. Mitra, Plenum Press, NY, 1979.

2. "Effect of Neutron Irradiation on the Pulse Dispersion in a Step-index Optical Fiber" by R. Rao and S.S. Mitra, Appl, Phys. Lett. 36, 948 (1980).

3. "Pulse Dispersion in Optical Fibers-Measurement Techniques and Radiation Effects" by R. Rao and S.S. Mitra in Physics of Fiber Optics, eds. B. Bendow and S.S. Mitra, Am. Ceramic Soc., Columbus, Ohio, 1981.

4. "Raman Scattering in Optical Fibers" by Guey-Lion Lan, P.K. Banerjee and S.S. Mitra, J. Raman Spectry, in Press.

We are grateful to Mr. F. DiMaglio and his staff at the R.I. Nuclear Science Center for their help in carrying out the experiments. Our thanks are also due to Dr. B. Bendow, Dr. R. Jaeger, and Mr. J. Wall for many helpful discussions.

i

TABLE OF CONTENTS

Page

Chapter 1

OPTICAL ABSORPTION SPECTRA OF NEUTRON IRRADIATED OPTICAL FIBERS IN THE 0.7 m TO 1.0 m REGION

ABSTRACT

The radiation induced attenuation in a number of optical fibers has been evaluated. Several different types of fibers were exposed to steady state nuclear radiation and the resulting decrease in transmitted power was monitored as a function of wavelength and radiation dose. The wavelengths examined were in the visible and near IR regions that are of specific interest for optical fiber communications. The fibers showed a decrease in transmitted power at all wavelengths examined. The radiation sensitivity in glass core fibers was observed to show dependence on factors such as impurity content and the index modifying dopants in the fiber.

INTRODUCTION

Previous investigations on the effects of radiation on optical fibers have shown the transmission through fibers to decrease on exposure to radiation [1-7]. These studies using primarily ionizing sources of radiation such as x-rays, gamma rays and pulsed neutrons have shown a great variation in sensitivity between different fiber types such as glass, plastic clad silica (PCS) and plastic fibers. In glass fibers, it has been observed that radiation sensitivity depends on factors such as impurity content [3], index modifying dopants [6] and drawing induced defects. A few studies of induced attenuation in fibers due to pulsed neutrons [7] have been done but a comparison of fibers under steady state neutron irradiation is not available even though there has been a continuing need for this information. These effects are particularly important to the military and also in applications such as in nuclear reactor control and monitor systems. Further-

more, energetic neutrons can produce a larger fraction of atomic displacement centers not observable after ionizing irradiation.

RADIATION PROCEDURE

The fibers were radiated at the 2MW research reactor of the Rhode Island Nuclear Science Center. When in operation the reactor core is a source of neutrons and gamma rays. The fibers were exposed to radiation in a beam port of the reactor. A 9 inch thick lead shield is located such that it can be raised or lowered within the beam port. When lowered most of the gamma radiation is attenuated, and exposure to primarily neutron radiation results.

Two heavy density concrete plugs, a smaller inner plug and a larger outer plug are used to shield the beam port. The fiber is wound on a spool which is attached to the inner shield plug. the ends of the fiber are threaded through helical holes in he plug in order to bring them outside. The plug is then inserted into the port. The ends of the fiber are then threaded through the outer shield plug which is inserted into the port behind the inner shield plug. Both ends of the fiber can thus be attached to measurement apparatus outside for in situ radiation measurements to be made.

The neutron flux of fast and thermal neutrons was measured by the reactor staff and found to be 3×10^6 N/cm^2/sec and 4.2×10^7 N/cm^2/sec, respectively. The gamma radiation was less than 400 r/hr with the 9 inch lead shutter down. the neutron fluence as a function of time is shown in Figure 1.

RESULTS

All results of radiation induced changes in attenuation are reported in db/km. The change in transmission was computed from the

relation.

$$\Delta T = \frac{1000}{L} \; 10 \; \log \frac{S_t}{S_o}$$

where S_t is the intensity of the transmitted signal taken at time t after commencement of the irradiation, S_o is the intensity of the transmitted signal before commencement of the irradiation and L is the length of fiber in m.

In all graphs a perpendicular line is drawn at the point where irradiation ceased. Readings taken beyond this point indicate the amount of recovery observed.

Figure 3 shows the relative change in attenuation of the ITT GS-02 fiber (P and Ge doped) for several different wavelengths. As can be seen, the response of the fiber in the visible is quite sensitive to radiation while in the IR it is less sensitive. Also, the radiation induced loss is very nearly linear for all wavelengths examined. No saturation was observed at the neutron fluence used. The recovery of the fiber an hour after irradiation is also shown. This shows that some annealing took place but a longer recovery time after irradiation is required to determine the final recovery level.

Figure 4 shows the relative change in attenuation of the ITT GG-02, Ge doped fiber. Again the response of the fiber in the visible was more sensitive to neutron irradiation than in the IR. However, the total change in attenuation was less than that of the fibers shown in Figure 3 and 5 which are doped with Ge and P. This indicates that the absence of P doping makes the radiation response of the fiber less sensitive to neutron radiation. The radiation response at 0.9 μm and 1.0 μm seemed to saturate at the highest doses presently used. Higher

3

doses are required in order to confirm this. This fiber was allowed to anneal for 16 hours after the irradiation and the results show little, if any, recovery. This indicates that without the P doping the damage incurred was relatively permanent.

Figure 5 shows the relative change in attenuation of an ITT GG-02 fiber with Ge and P doping. Here, too, the response of the fiber in the visible was more sensitive to neutron radiation than in the IR. The fiber was more sensitive at all wavelengths observed than the GG-02 fiber of Figure 4 which did not have P doping. Again the addition of P appeared to make the fiber more sensitive to neutron radiation.

Figure 6 shows the relative change in attenuation of an ITT plastic clad silica fiber (PS-05). Initially, the radiation response at all wavelengths rose sharply but then a point was reached where the response seemed to saturate and for 0.8 μm and 1.0 μm it decreased. Finally, the loss increased rapidly at higher doses. This fiber was allowed to anneal for 88 hours after irradiation and the results showed a substantial amount of recovery. The decrease in the fibers attenuation at 0.8 μm and 1.0 μm while the fiber was being irradiated appears to be inconsistant with results obtained on other fibers. The cause could have been due to a fluctuation in the monochromator output intensity.

Figure 7 shows the relative change in attenuation of a QSF-200, 200 μm core plastic clad silica fiber. This fiber has a lower OH content than the PS-05 fiber described above. The response at all wavelengths was fairly linear with greater sensitivity in the visible than in the IR. Overall sensitivity to radiation was the lowest of all the glass fibers examined. At 0.9 μm the relative change was less than 10 db/km

4

after 5 hours of irradiation.

In a second study, the QSF-200 fiber was exposed to a much greater flux of neutrons and dose of gamma rays. This was done by raising the lead shutter which is located between the reactor core and the sample location. The neutron fluence in the 10 minutes of irradiation shown with the shutter open, was greater than the fluence in 7 hrs. of irradiation with the shutter closed. On opening the shutter with the monochrometer set at 860 nm, the power output from the detector showed an exponential like decay. This is shown in Figure 8. After 10 minutes, the response of the fiber appeared to have been saturated. The total change in attenuation in the 10 minute span was 77 db/km and the total attenuation from the pre-irradiation levels was 81 db/km. Table 1 shows the induced attenuation at different wavelengths from pre-radiation levels. After a half hour of irradiation, the shutter was lowered and the output of the fiber showed an exponential like recovery. This is shown in Figure 9. The recovery rate was slower than the decay rate. In the first 26 minutes of recovery, the attenuation changed by 60 db/km.

Figure 10 shows the relative change in attenuation of a medium loss plastic clad silica fiber with a core diameter of 250 μm. This fiber's sensitivity is in sharp contrast to the other PCS fibers. It showed much higher changes in attenuation than any other fibers examined. The high impurity content of this fiber core appears to be responsible for the extreme sensitivity. After 4 hours of irradiation the signal was too weak to be observed and no further data was taken. No annealing was observed either, after irradiation ceased. Again the attenuation in the visible was more significant than in the IR.

5

Figure 11 shows the relative change in attenuation for an IRT plastic fiber. This fiber was examined in the wavelength region from 0.6 μm to 0.84 μm. Unlike the glass fibers the attenuation was more significant in the IR than in the visible. The change in attenuation for all wavelengths was a small percentage of the fiber's total unirradiated attenuation levels. The radiation response saturated relatively early during irradiation. For all wavelengths examined, the fiber recovered completely.

OBSERVATIONS

All the glass fibers and PCS fibers showed greater sensitivity to neutron irradiation in the visible wavelengths than in the IR wavelengths examined.

The glass fibers with phosphorous and germanium doping were more sensitive to radiation than the fiber without phosphorous. However, the fibers with phosphorous showed some recovery whereas the fibers with germanium doping showed no recovery.

Of the glass fibers the high purity glass core plastic clad fibers were the least sensitive fibers to radiation. The PCS fibers employing high purity cores showed indications of complete recovery. The rapid growth and decay of induced attenuation shown in Figures 8 & 9 indicate the damage incurred by PCS fibers are of a more temporary nature than that in the doped glass fibers. The medium loss PCS fiber had extremely high induced losses probably due to its high impurity content.

Unlike the glass fibers the plastic fiber was more sensitive in the IR than in the visible and also showed complete recovery after irradiation.

6

REFERENCES

1. J.A. Wall and J.F. Bryaht, "Radiation effects on fiber optics," Physical Sciences Research Paper No. 627, AFCRL, Hanscom AFB, Mass., April 2, 1975.

2. E.J. Frieble, G.H. Sigel, Jr. and R.E. Jaeger, "In-situ measurement of growth and decay of radiation damage in fibe optic waveguides," presented at topical meetings on Optical Fiber Transmission II, Williamsburg, Va., Feb. 22-24, 1977.

3. E.J. Frieble, R.E. Jaeger, G.H. Sigal, Jr., and M.E. Gingerich, Appl. Phys. Lett. 32, 95 (1978).

4. B.D. Evans and G.H. Sigal, Jr., IEEE, Trans. on Nuclr. sci. 22, 2462 (1975).

5. M.K. Barnoski and B.D. Evans, Proc. of the IEEE 66, 423 (1978).

6. E.J. Frieble, M.E. Gingerich, and G.H. Sigel, Jr., Appl. Phys. Lett. 32, 619 (1978)

7. P.C. Mattern, L.M. Watkins, c.D. Skoog and E.H. Barsis, IEEE Trans. on Nuclr. Sci. 22, 2468 (1975).

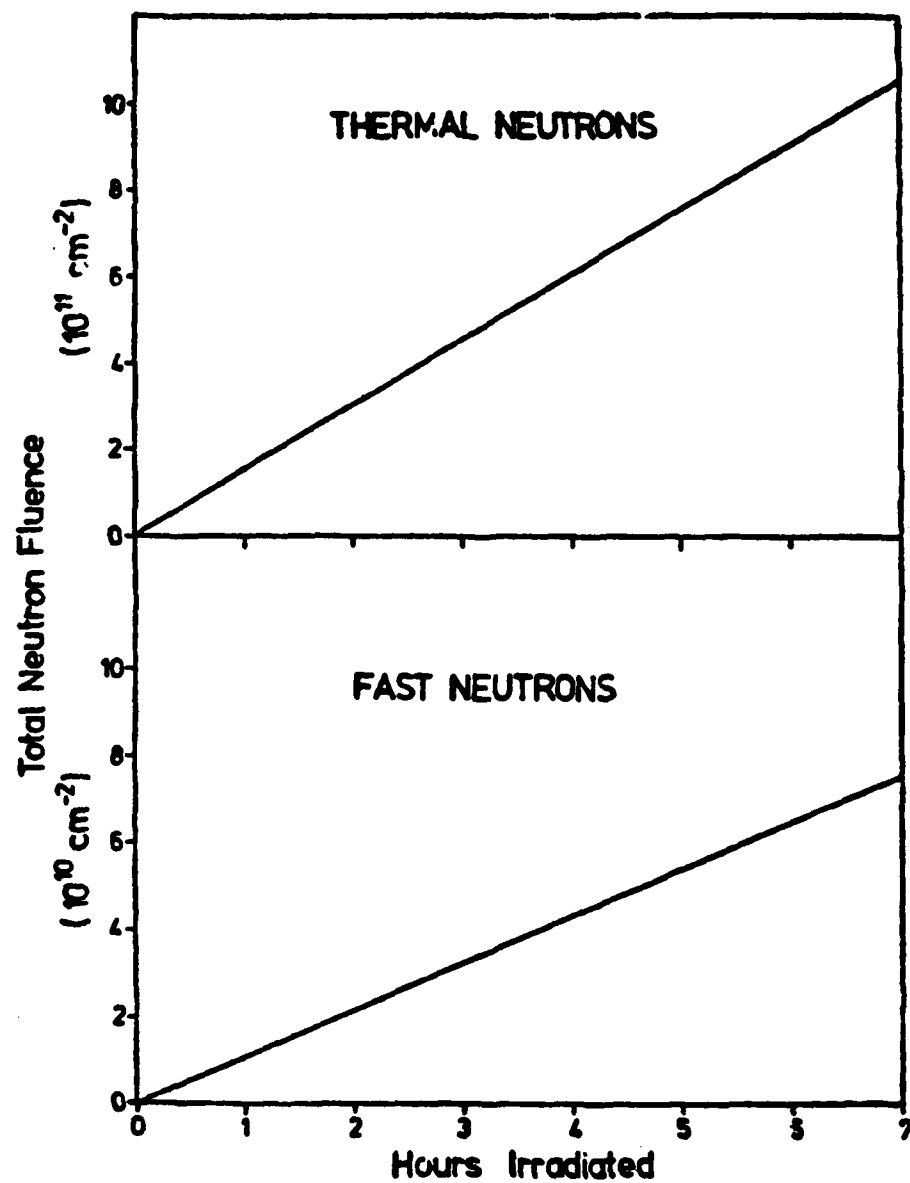8. P.K. Bandopadhay, Nuclr. Inst. and Methods. 94, 125 (1971).

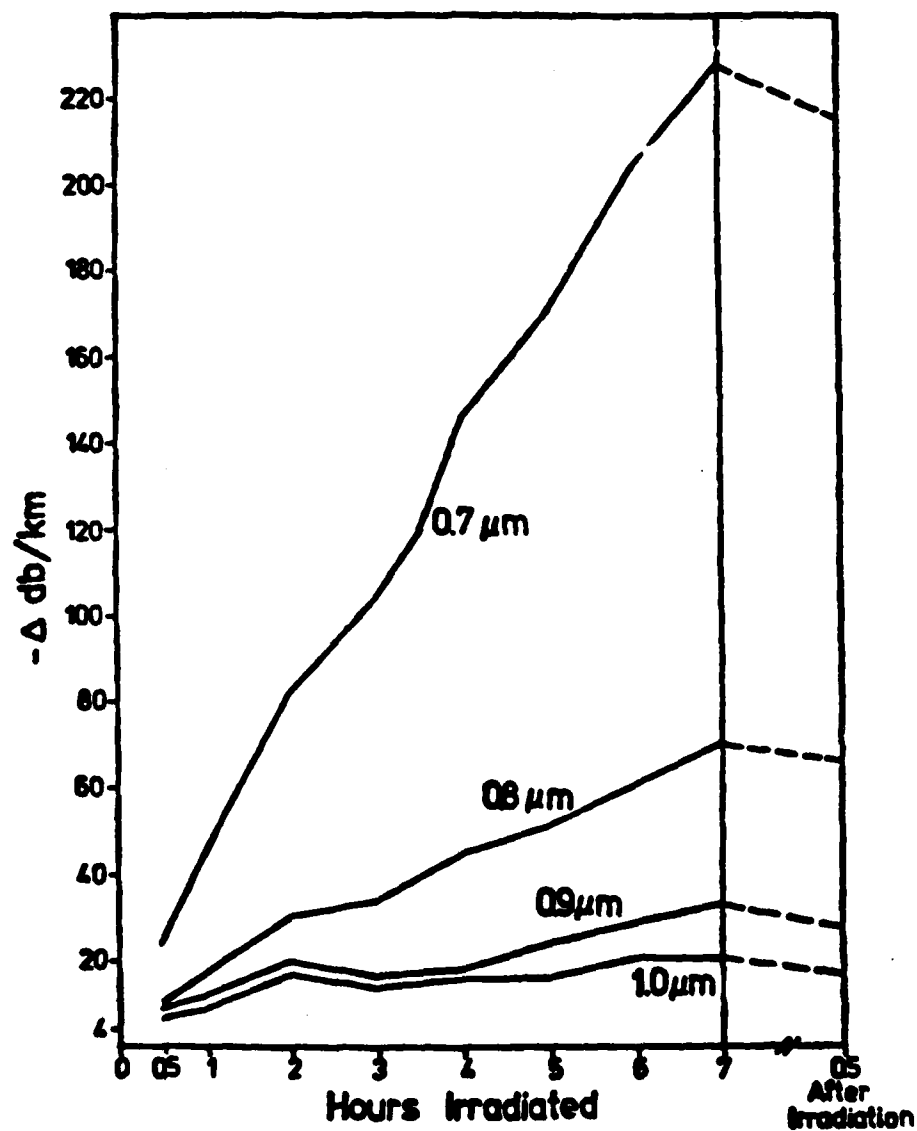Figure 1. Total neutron fluence vs. time of irradiation

8

Figure 2. Change in attenuation vs. time of irradiation ITT GS-02, 55 μm Core, Step Index, Ge and P Doped, Low OH Content Fiber.

9

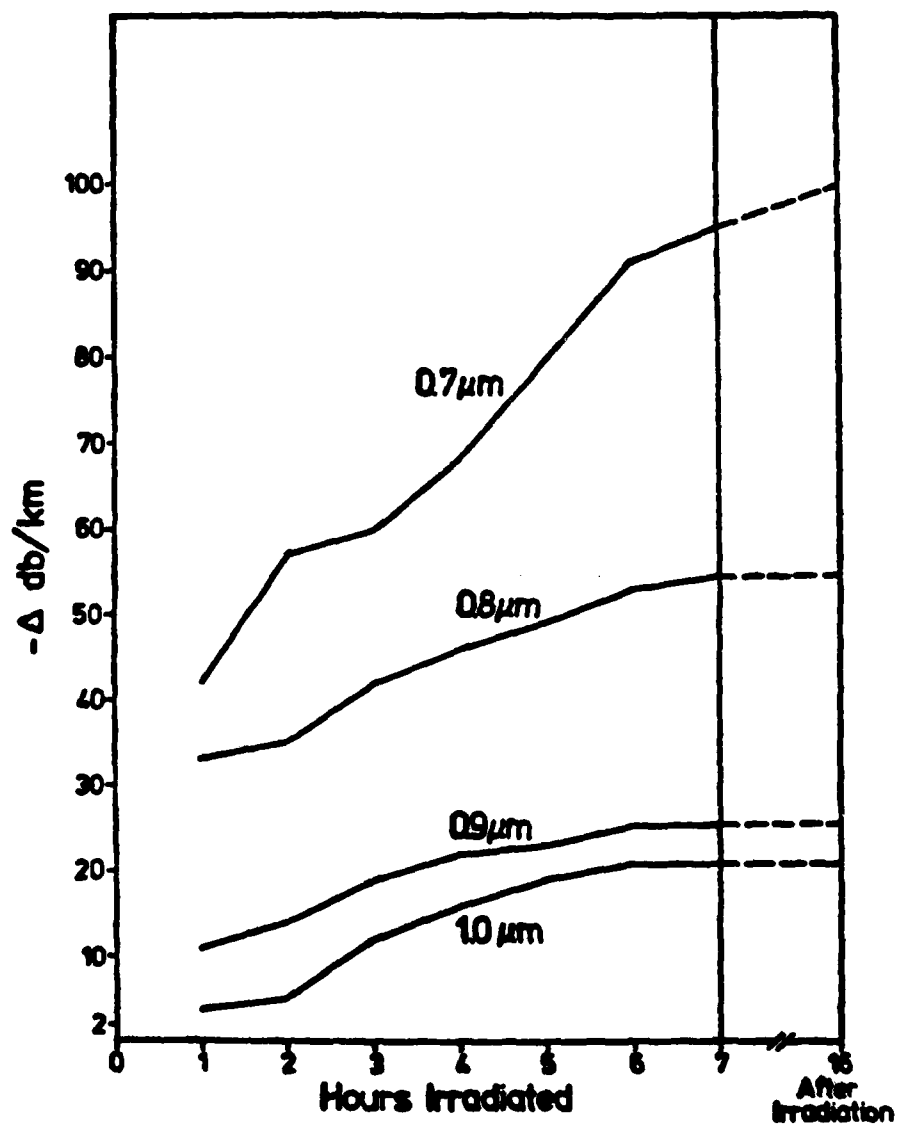Figure 3. Change in attenuation vs. time of irradiation.
ITT GG-02, 50 μm Core, Graded Index, Ge Doped,
Low OH Content Fiber
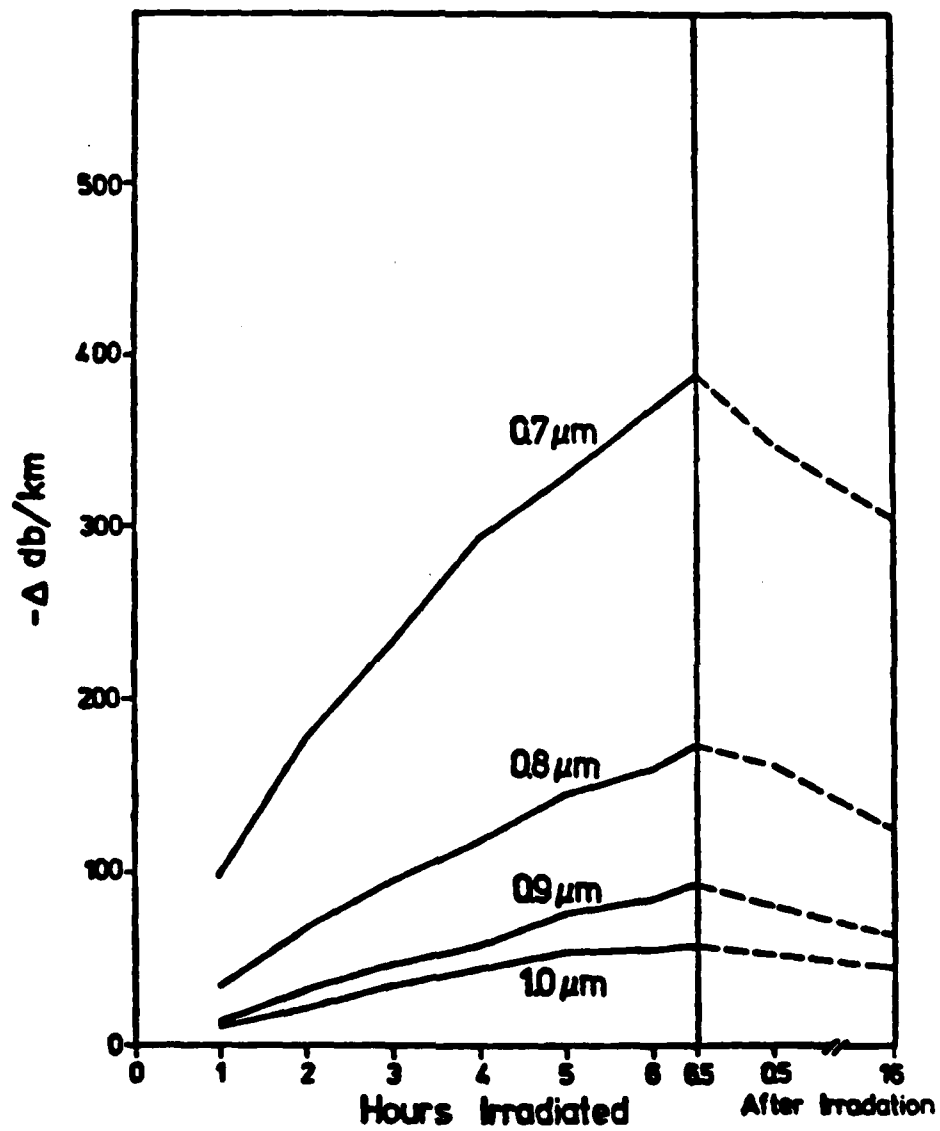
Figure 4. Change in attenuation vs. time of irradiation ITT GG-02, 50 μm Core Graded Index, Ge and P Doped Low OH Content Fiber.

11

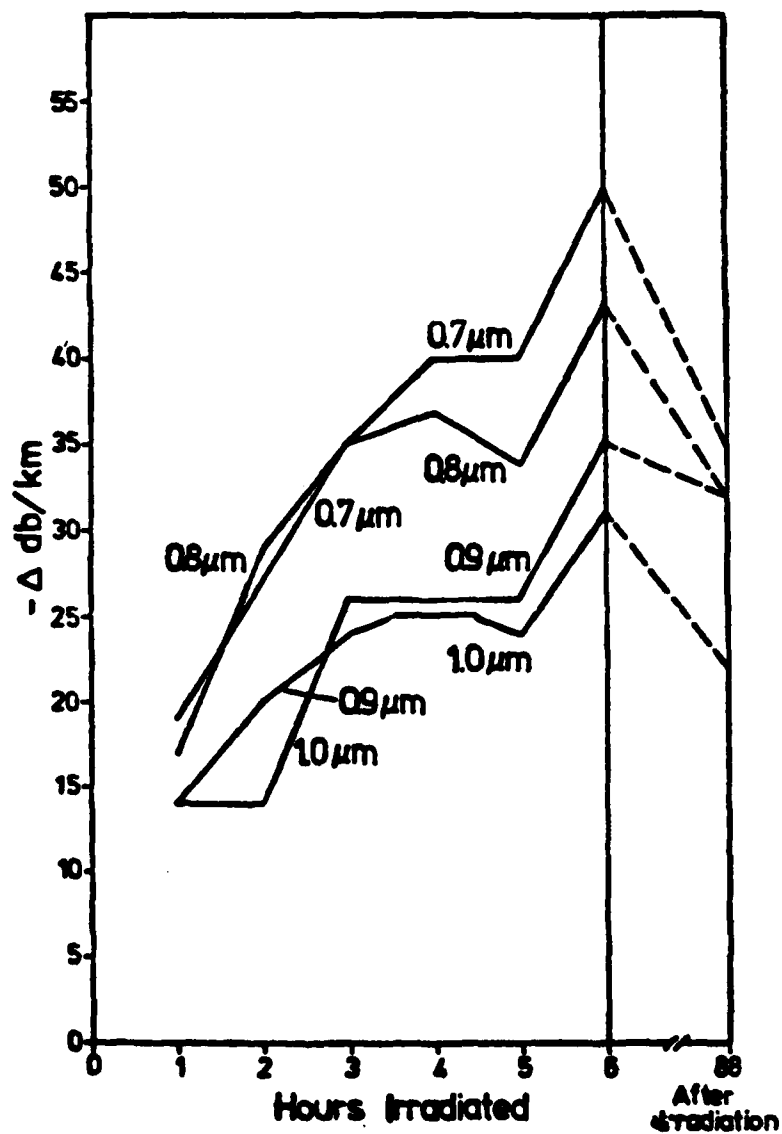Figure 5. Change in attenuation vs. time of irradiation. ITT PS-05, 125 μm Core Plastic Clad Silica, High OH Content Fiber.
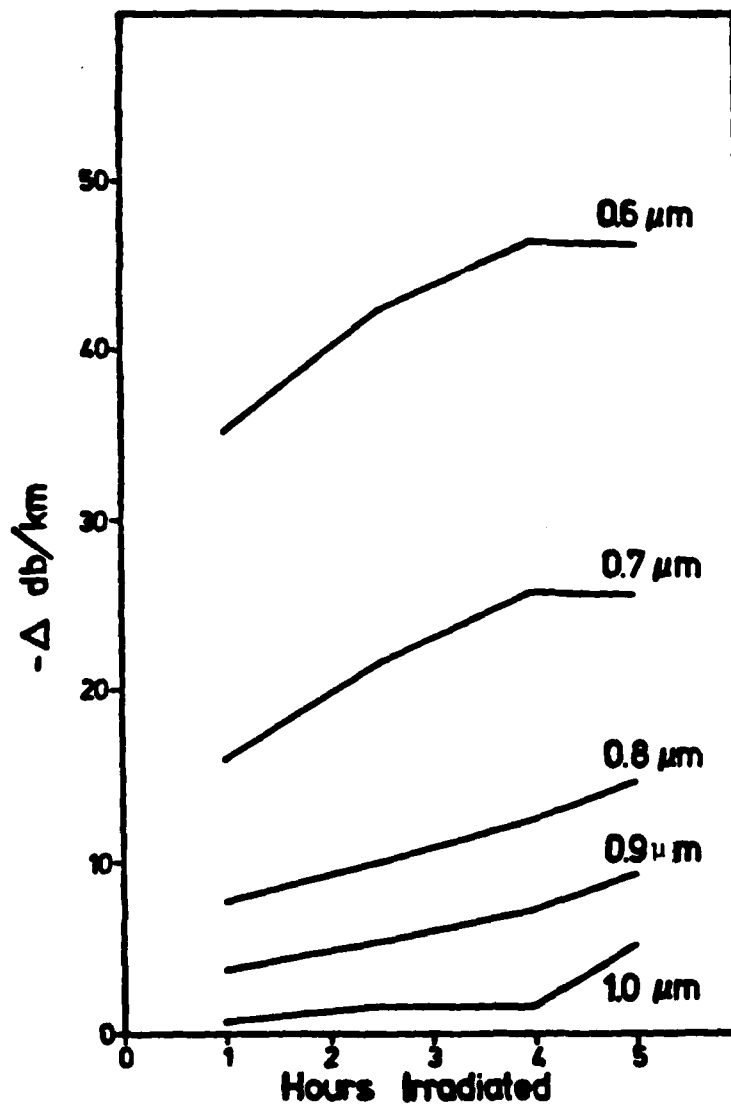
12

Figure 6.   Change in attenuation vs. time of irradiation,
            QSF-200 200 µm Core Plastic Clad Silica, Low OH
            Content Fiber.

13
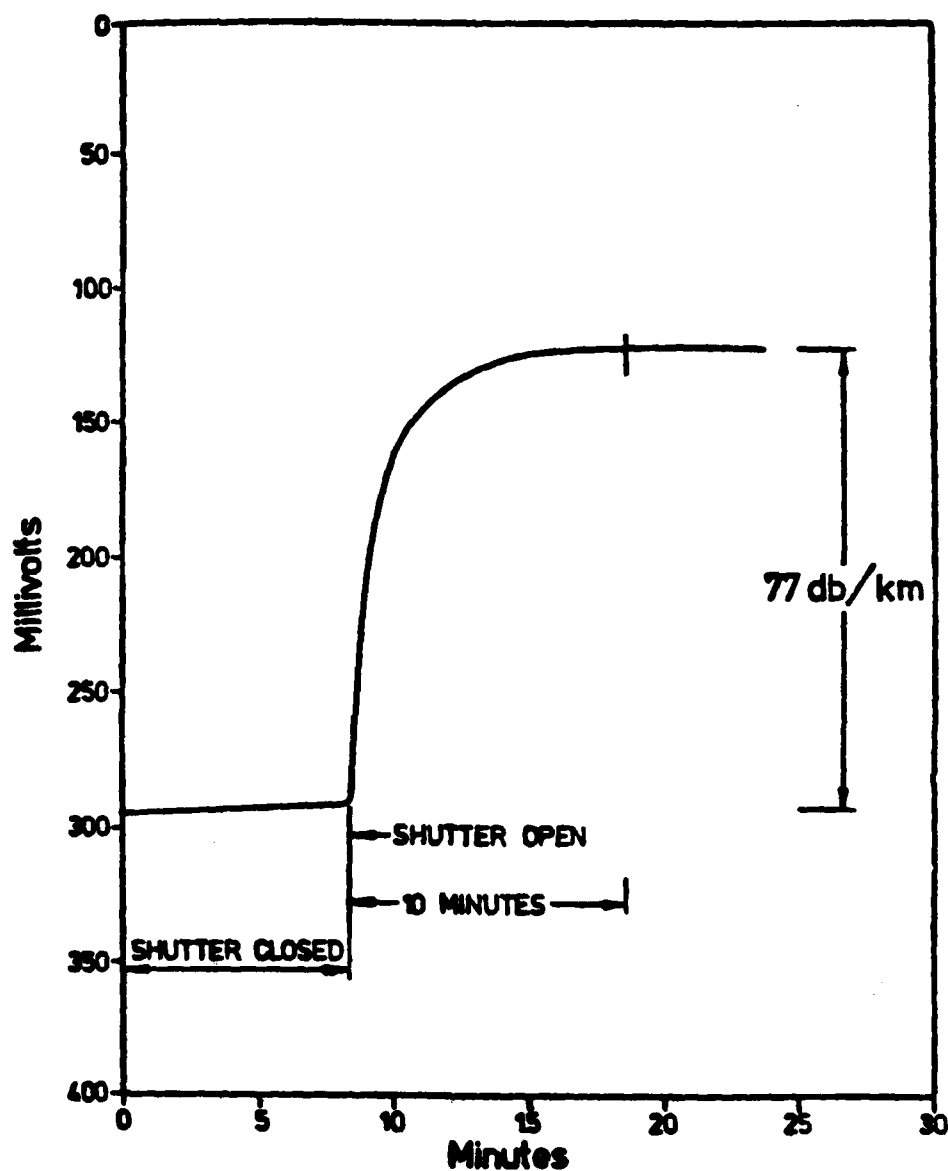
Figure 7. QSF-200 fiber output on opening the lead shutter and subjecting the fiber to much a greater flux of neutrons and dose of gamma rays.

14

λ(nm)	Δ(^{db}/km)
800	295.4
700	190.9
800	115.2
860	81.0
900	64
920	58.5
990	40.5
1000	33.6

Table 1. Total change in attenuation of QSF-200 after exposure to a much greater flux of neutrons and dose of gamma rays.

SHUTTER
OPEN

SHUTTER CLOSED

0 —

50 —

Millivolts

100 —

150 —

60 db/km

200 —

250 —

300 —

0   5   10   15   20   25   30

Minutes

Figure 8.   QSF-200 fiber output on closing the lead shutter.

Figure 9. Changes in attenuation vs. time of irradiation.
Rank 250 μm Core Plastic Clad Silica, Medium
Loss, High OH Content Fiber.

17

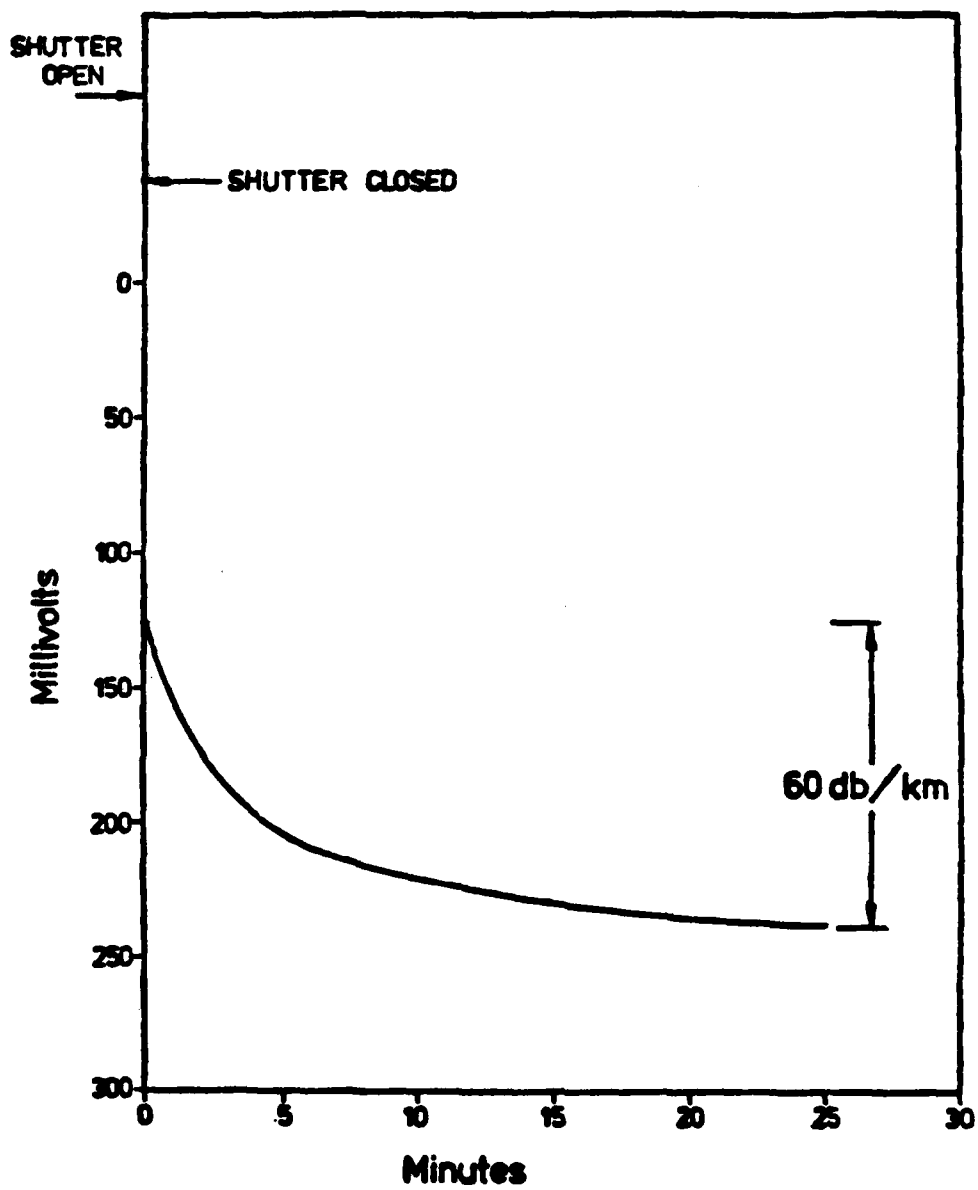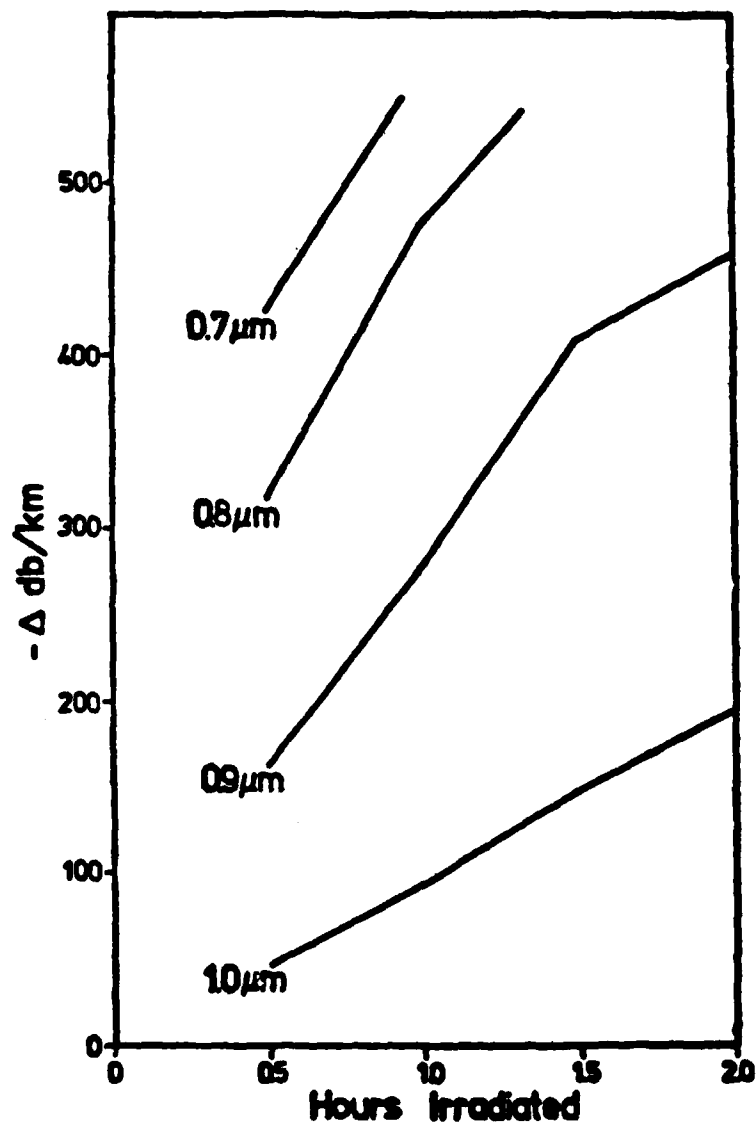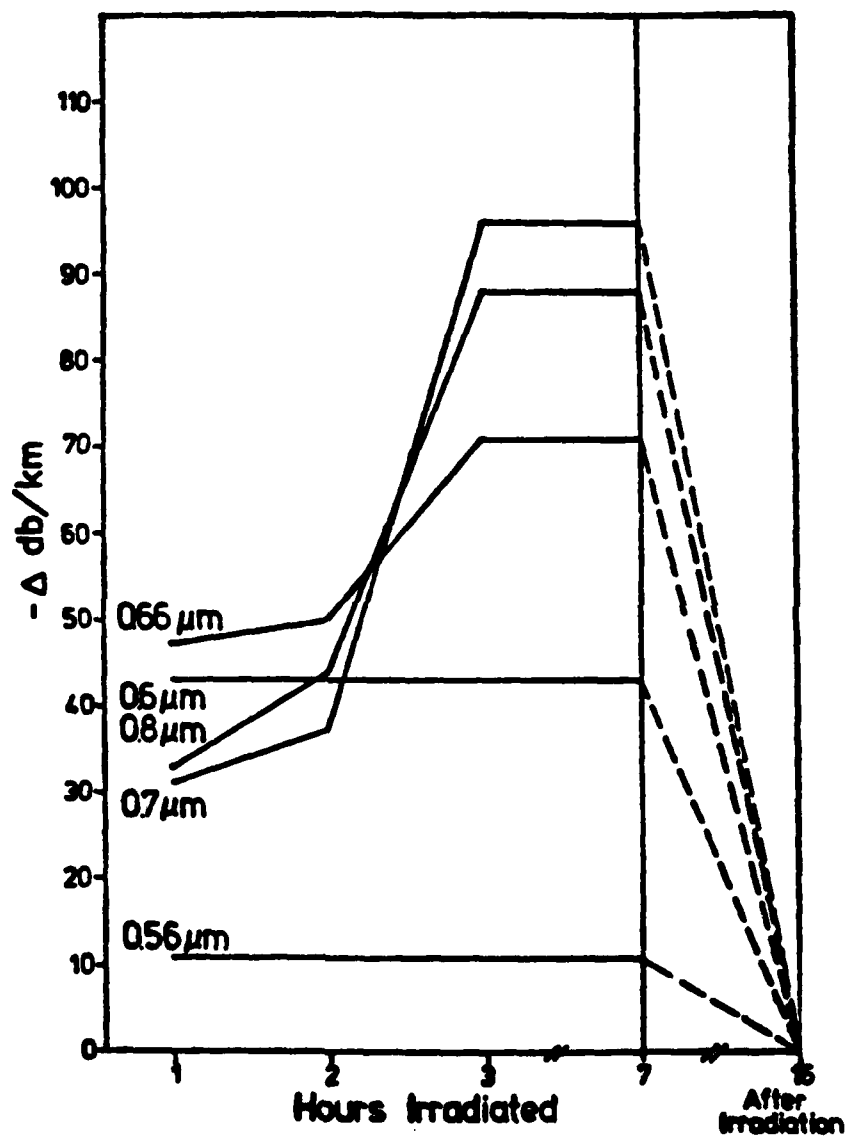Figure 10. Change in attenuation vs. time of irradiation. IRT plastic fiber.

18

Chapter 2

EFFECT OF NEUTRON RADIATION ON THE PULSE DISPERSION IN A STEP INDEX OPTICAL FIBER

Abstract

Experimental measurements of neutron radiation induced pulse dispersion changes, and attenuation changes in a 100 μm core step index fiber were made. In the course of irradiation pulse dispersion in the fiber was observed to decrease while the attenuation increased. The results indicate greater decreases in the transmission of higher order modes. This reflects the fact that the radiation response of a fiber is determined by the respective refractive indices and absorption coefficients of both the core and cladding of the fiber. Results are presented along with a discussion of mechanisms by which dispersion changes can occur in irradiated fibers.

Introduction

Many studies on the effects of radiation on optical fibers have dealt with the radiation induced attenuation [1,2,3,4] and fluorescence [5] that occur in fibers. In some studies the radiation induced absorption in bulk glass samples that are used in making fibers has been examined [5,6]. Though from these studies it is evident that pulse broadening or bandwidth changes can occur in irradiated fibers such a study has not been made.

The objectives of this study were to (1) investigate whether the pulse dispersion (bandwidth) of an optical fiber can be affected in a radiation environment, and (2) gain further insight into the mechanisms by which loss of transmission occur in irradiated fibers. The results show that pulse broadening changes do occur, and when examined in the

19

light of theoretical considerations suggest that preferential mode attenuation is the cause of the changes. A discussion of the mechanisms by which radiation induced changes in pulse dispersion occur is also presented.

Dispersion Change Mechanisms

Absorption changes in glass which are associated with light emitting and absorbing defect centers generated by radiation are known to depend on several factors such as trace impurities and index modifying dopants. Core dopants in particular have been shown to be an important factor in the sensitivity of glass fibers to neutron radiation. The composition of the core and cladding of an optical fiber differ to satisfy the requirement of having an index difference and could consequently undergo different changes in their absorption coefficients when irradiated. This indicates that a change in pulse dispersion of a fiber can occur. An increase in the absorption coefficient reflects a change in the imaginary part of the complex refractive index. The real and imaginary parts of the refractive index are dependent on each other as described by the Kramer Kronig dispersion relations. The radiation induced increase in the absorption coefficient of a glass is thus accompanied by a corresponding change in the real part of its refractive index. In the case of an optical fiber, this would result in a change in V, the normalized frequency of the fiber defined as[7]

$$V = \frac{2\pi a}{\lambda} \; (n_1{}^2 - n_2{}^2)^{1/2}$$

where a is the radius of the fiber core, n_1 and n_2 are refractive indices of the core and of the cladding respectively. Plots of V vs.

these parameters reveal that shifts in the V value can alter cut off points resulting in the escape of some higher order modes, or in an increase in the number of guided modes. This effect can alter the group dispersion in a fiber. Furthermore, since the field of a guided mode extends into the cladding of a fiber [7], the absorption coefficient for a given mode is a function of the absorption of both the core and cladding and also the power distribution within the core and cladding. For a given V, the ratio of power in the cladding to the total power in the mode is greater for higher order modes. Relatively higher changes in the absorption coefficient of the cladding would result in greater attenuation of higher order modes [8]. This would reduce the number of modes transmitted and thus would affect the group dispersion.

Experimental Technique

The experiments were carried out at the 2 MW research reactor of the Rhode Island Nuclear science Center. When in operation, the reactor core is a source of neutrons and gamma rays which irradiate samples placed in the beam port of the reactor. A nine inch thick lead shield within the beam port was lowered to attenuate the gamma rays while allowing neutrons to pass through. Two aluminum plugs were used to close the port and prevent radiation from escaping to the outside. The fiber sample was placed behind the lead shield and its ends were threaded through helical holes in both plugs and attached to the measurement apparatus outside. In-situ pulse width measurements were made while the fiber was being irradiated with neutrons.*

---

*The radiation procedure is described in greater detail in manuscript #1

A 200 ps optical pulse is generated in a GaAs laser at 904 nm and then collimated and launched through a 10xmicroscope objective into the fiber. The output from the other end of the fiber is focused by a lens on a high speed silicon detector. A variable beam splitter is placed in between the focusing lens and the detector. This enables a second detector to provide a trigger to the sampling oscilloscope. In the course of irradiation, the pulse amplitude falls considerably due to induced attenuation. The variable beam splitter in conjunction with the oscilloscope gain, facilitates the adjustment of the pulse to any height on the scope. All readings of pulse width and rise time can thus be taken with essentially a fixed pulse amplitude on the scope. The fiber used for the experiment was a Galileo 100 μm core step index fiber with phosphorous and germanium doping. The pulse dispersion measurement equipment is described in greater detail in Appendix #2.

Results and Discussion

With one m of fiber, the detected pulse had a rise time of 400 ps and a FWHM pulse width of 840 ps. With the 500 m of fiber used for the irradiation, the detected pulse before irradiation had a rise time of 1.2 ns and a FWHM pulse width of 5.1 ns. As irradiation progressed, the pulse width gradually narrowed. Figure 1 shows the change in FWHM pulse width as a function of time. After 8 hours of irradiation, the width had decreased to 4.5 ns. At the same time, the rise time of the pulse remained unchanged at 1.2 ns. Figure 2 shows the change in attenuation over the same period of time normalized to 1 km. It is observed that the attenuation change was fairly linear with time with a total change of 17 db/km after 8 hours of irradiation. For both cases

22

pulse dispersion and attenuation, a saturation level did not occur for the radiation levels used. The fiber was allowed to recover for a period of 48 hours after irradiation. The FWHM pulse width recovered to 4.65 ns and the attenuation went down to total change of 13.62 db/km in relation to pre-irradiation levels.

Neutron radiation is observed to effect the pulse dispersion in optical fibers. Narrowing of the pulse can be attributed to the loss of higher order modes. This could have occurred due to one or both of the following reasons (1) Refractive index changes caused a shift in V to a lower value resulting in the escape of higher order modes and/or (ii) Extreme absorption was induced in the cladding resulting in the loss of higher order modes by attenuation The low order modes were not effected significantly, if at all. This is indicated by the fact that the rise time or leading edge of the pulse did not change. For the irradiation levels used in this study the dispersion changes were small. Since the dispersion decreased, the fiber bandwidth in effect increased. Unlike the dispersion change, the attenuation change was significant possibly making the latter change a more important consideration in the deployment of fiber optic systems in radiation environments.

The study also demonstrates that an interrelation between pulse dispersion and attenuation changes due to radiation may exist. Specifically the escape or the absorption of higher order modes resulting in reduced group dispersion also results in less transmitted power. It is apparent that both the core and cladding of a fiber play a part in the loss mechanisms that occur during radiation, and that cladding composition may be an important consideration in the design of a radiation

23

resistant fiber.

References

1. J.A. Wall and J.F. Bryant, "Radiation effects on fiber optics," Physical Sciences Research Paper No. 627, AFCRL, Hanscom AFB, Mass., April 2, 1975.

2. E.J. Frieble, G.H. Sigel, Jr., and R.E. Jaeger, "In-situ measurement of growth and decay of radiation damage in fiber optic waveguides," presented at Topical Meeting on Optical Fiber Transmission II, Williamsburg, Va., Feb. 22-24, 1977.

3. E.J. Frieble, R.E. Jaeger, g.H. Siegal, Jr., and M.E. Gingerich, Appl. Phys. Lett. 32, 95 (1978).

4. B.D. Evans and G.H. Sigal, Jr., IEEE Trans. on Nuclr. Sci. 22, 2462 (1975).

5. M.K. Barnoski and B.D. Evans, Proc. of the IEEE 66, 423 (1978).

6. G.H. Sigal, Jr. and B.D. Evans, Appl. Phys Lett. 24, 410 (1974).

7. D. Gloge, Appl. Opts. 10, 2252 (1971).

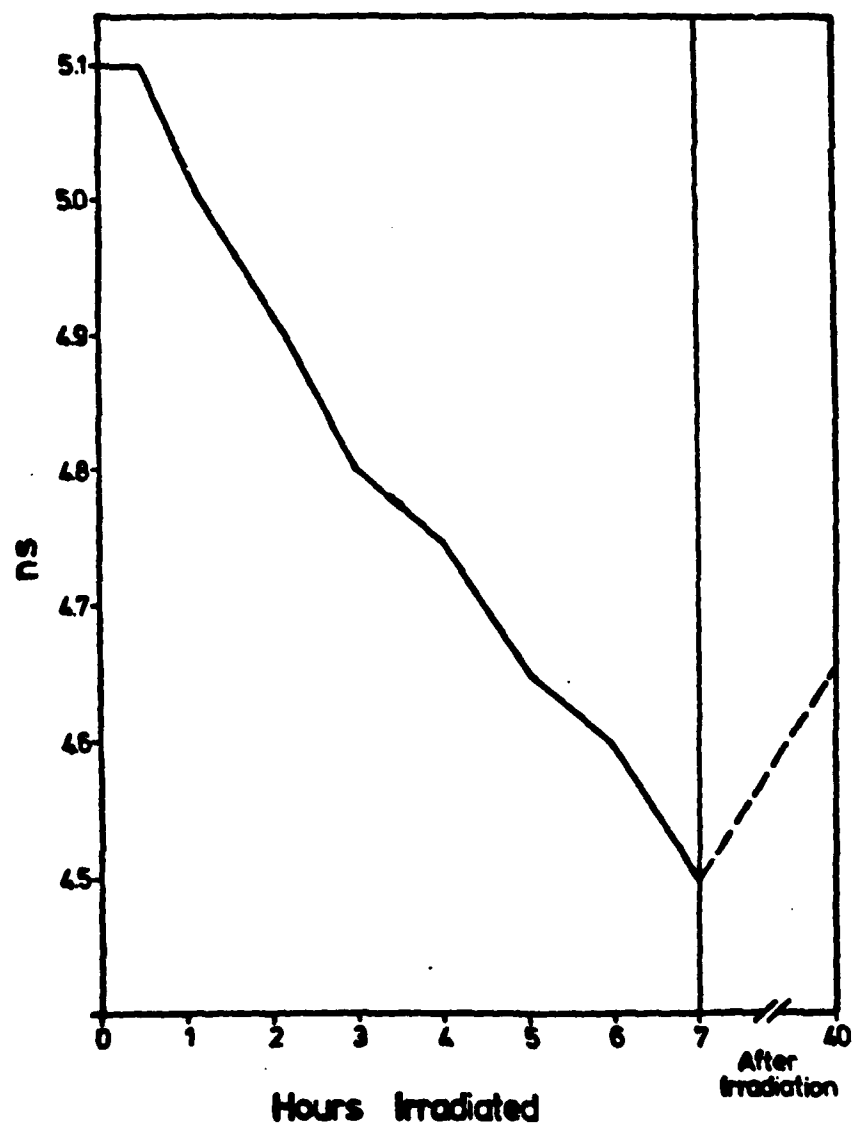8. A.N. Snyder and J.D. Love, Electron lett, 12, 255 (1976).

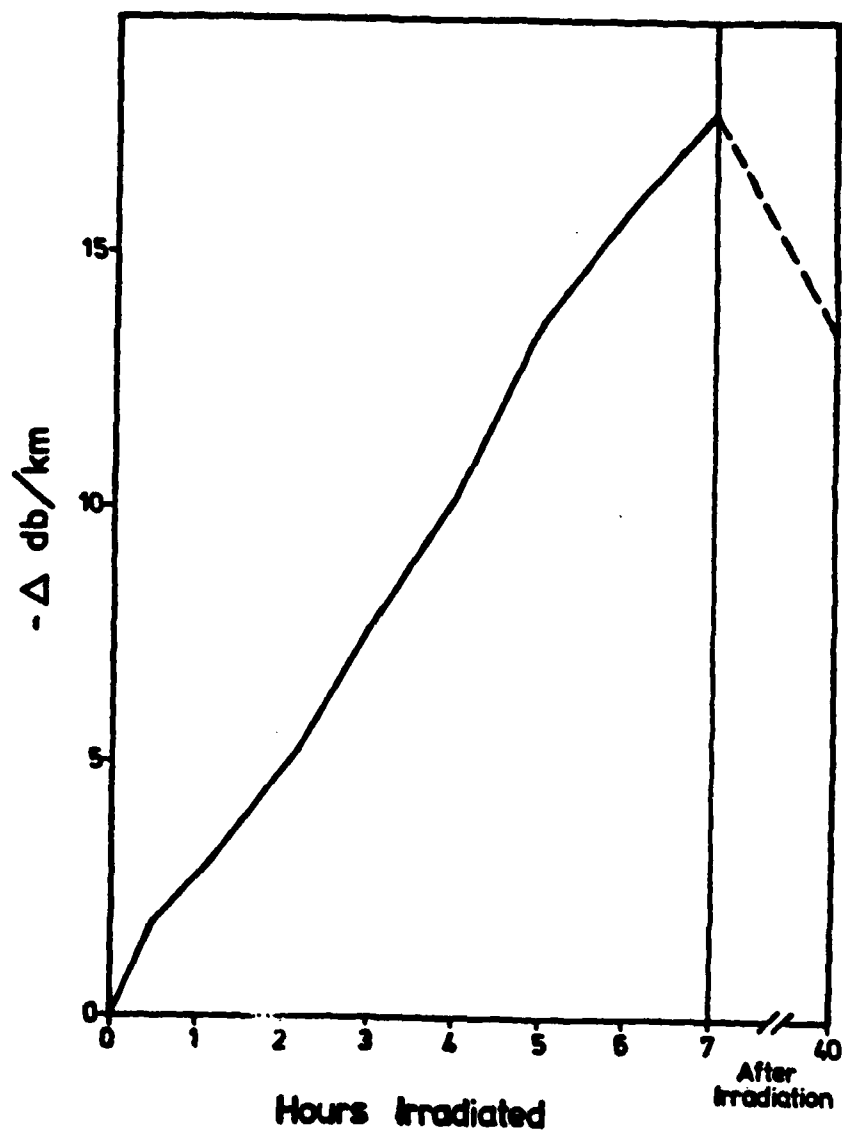Figure 1. Pulse dispersion vs. time of irradiation.

25

Figure 2.   Change in attenuation vs. time of irradiation.

Chapter 3

RAMAN SCATTERING IN OPTICAL FIBERS

Abstract: In this paper we review the light scattering spectra
of optical fibers and present new data on Raman Spectra of optical
fibers. The results include Raman Spectra of fused Silica fibers
and effects of dopants and irradiation. Large scattering volumes
available in optical fibers afford one to detect low dopant
concentrations and relatively weak second order spectra. Low
frequency Raman Spectra of optical fibers shows the expected
non-Debye type anomoly.

INTRODUCTION

Application of low-loss high bandwidth fibers in communication systems offer many significant advantages compared with traditional cables, which include   high available bandwidth, longer repeater seperation, inductive interface and ground-loop immunity, less susceptible to nuclear radiation effects and faster recovery, no cross-talk, small size and light weight, and potentially less expensive.

In this paper, we present a detailed review on light scattering in optical fibers and briefly discuss polarization effects. Experimental data on Raman scattering of single and multi-mode optical fibers of pure and doped fused silica are presented and discussed in terms of fiber configurations and dopants.

SiO_2 glass is the most general optical fiber material, and doped SiO_2 fibers exhibit a broad transmission window for optical communication. GeO_2 is the principal dopant in most waveguide designs. Because of its high temperature characteristics, B_2O_3 or P_2O_5 is always used as a softening agent to facilitate preform fabrication by any of the three vapor phase processing methods.[1] Considerable amount of research has been done on Raman spectrum of bulk samples of optical glass but the spectrum reported from optical fibers is still very limited[2-6].   Raman spectrometric method is developed as a non-destructive in-situ method of characterizing optical materials and devices. It has been known that the Raman

28

spectrum is sensitive to small amounts of additives. Thus this technique is applicable to evaluate the compositions of fiber material glasses. Scattering from long lengths of fibers differ considerably from conventional perpendicular scattering geometry. Low loss optical waveguides are capable of guiding electromagnetic waves over long distances and confining it to a small cross-sectional area. Maintaining high optical power densities over long material interaction lengths, results in an intensification of the Stokes output[2,4,7]. Thus, some extremely weak features which can not be observed by conventional 90° scattering is now observable in fibers[4] (and see also Fig. 4.).

Another advantage of fiber Raman spectrum is that it becomes possible to study glass composition in fibers which otherwise would not be stable in large bulk samples, and also small quantities of liquids can be studied in hollow fibers. In addition, nonlinear optical effects like stimulated Raman and stimulated Brillouin scattering can be obtained in rather low threshold power and these effects are applicable to tunable fiber Raman lasers[7-11]. In this paper, however, attention will be focussed only on the spontaneous Raman scattering in optical fibers.

One of the disadvantages of fiber Raman spectroscopy is caused by the fact that the excitation line is coupled into the spectrum along with the Stokes output. This situation prevents discrimination of low frequency Raman bands from the strong background of the excitation line. With very narrow slit widths, however, it is

29

possible to scan to rather low frequencies suitable for most purposes.
Very close to the excitation line, grating ghosts become a very
serious problem, because, here the intensity of output light due to
both Stokes and pump power is high and narrow slit width improves the
resolution. Grating ghosts could be identified by a pair of narrow
band interference filters past the laser line. One method is to
first put both the filters on the entrance of the fiber and compare
this spectrum with that obtained by putting one filter on the fiber
entrance and the other on the fiber output end. Ghosts should appear
with equal intensity in both spectrum while Raman lines will not
appear in the second spectrum.

Linear polarization output in optical fibers is essential for
utilization of polarization dependent devices[12], and can reduce
the threshold power by a factor of two in fiber Raman and Brillouin
lasers[13]. Unfortunately, most fibers scramble the polarization,
thus making investigation of polarised Raman spectra in optical fibers
a very difficult task. Because of irregularities in geometry and
refractive index, the energy originally in the dominant mode becomes
quickly distributed equally among all possible propagating modes. A
small phase velocity difference between modes will significantly
distort the phase of a wave after propagating a short distance and
lose the polarization. By the above assumption, depolarization in
fibers is caused by phase difference between modes. It seems only
single mode fibers can maintain the polarization, and, in general,
polarization output may be obtained in very short length fibers.

EXPERIMENTAL METHOD

In our work with fiber Raman scattering we have used the 6328A$^{\text{o}}$ line of a He-Ne laser and 4880A$^{\text{o}}$ and 5145A$^{\text{o}}$ lines of an Argon-ion laser as exciatation sources. Raman Spectra were analyzed by a Spex Industries Model 1400 double monochrometer with a photon counting detection system. Walrafen, et al[6] have used Cary Model-81 spectrometer and 4765A$^{\text{o}}$ Argon-ion laser radiation instead of the more intense radiations at 4880A$^{\text{o}}$ and 5145A$^{\text{o}}$. The laser light in our set up is focused onto the fiber by microscope objectives with numerical apertures (NA) lower than that of the fibers in order to couple the laser output into the fibers. The fiber could be mode stripped by immersing a small length of the fiber near the input and output ends in glycerine bath mode strippers or simply painting a short length of bare fiber at both ends with black paint to remove any radiation trapped by total reflection at the cladding-air interface[2,14].

For obtaining more information from cladding, in some experiments, we have used microscope objectives with NA somewhat higher than that of the fibers. Input end of the fiber is mounted by a three-dimensional micromanipulator or a vacuum chuck on a three dimensional stand. The input laser spot and waveguide core are aligned by a viewing telescope. End preparations of the fibers are preformed by standard techniques, such as obtaining optically flat faces perpendicular to the fiber axis. Ends are then examined by a microscope. Another method to examine cuts and input alignment is done by projecting the fiber output pattern on

a screen. If the cuts are flat enough and input laser light is exactly focused on the core, the pattern should be an almost perfect circular speckle while 'bad' ends project distorted pattern. Light coupled from the cladding results in an outer circle around the internal pattern. An absorption filter or an interference sharp cut filter could be inserted between the output end of the fiber and the spectrophotometer in order to reduce the pump power coupling into output light thus improving resolution. This also allows examining the spectral region closer to the excitation line[6]. The output light from the fiber is either collected by a camera lens and then focused on the spectrometer entrance slit or by using the fiber output end directly shining onto the entrance slit.

EXPERIMENTAL RESULTS AND DISCUSION

Pure SiO_2 Core Fibers:

The Raman spectrum of pure-SiO_2 core fibers was obtained from a 20-meter, Rank PCS-1 plastic clad silica fiber with medium loss, high OH content, 250 μm pure SiO_2 core and 0.24 NA. The 6328A^o excitation line of a Spectra Physics model 125 He-Ne laser (and, in some cases, using the 4880A^o excitation line of Model 52 G Coherent C4, Argon-Ion laser) was used. The beam was focused by a 20 X microscope eye piece with 0.45 NA, which is larger than that of the fiber in order to collect more information from the plastic cladding. The output light of the fiber was collected by a camera lens focused onto the entrance slit. The entrance slit was carefully shielded from all light except that coming from the output end of the fiber. The resultant spectra are shown in Figs. 1 and 2 for the

frequency ranges 10 cm^{-1} to 1300 cm^{-1} and, 1300 cm^{-1} to 3000 cm^{-1}, respectively. Figs. 3 and 4 show the Si-OH and OH stretching modes. The data are tabulated in table I and compared with those reported on bulk SiO_2 samples[15,16]. Our results show that the locations of Raman peaks on fibers and bulk samples are very close to each other. Slight shift can be attributed to the uncertainty caused from the broad peak characteristics of glasses, the instrumental uncertanity and the fact that the spectra of fibers are the combination of polarized and depolarized part of output light which should be slightly different from just polarized part reported in reference (15) and (16). Vitreous silica has long been considered as a continuous network of nearly perfect SiO_4 tetrahedra connected to each other. The characteristic disorder in a silica glass is usually described in terms of large variations in the orientation of neighboring tetrahedra[15,17]. The peak frequencies at 450 cm^{-1}, 800 cm^{-1}, 1055 cm^{-1} and the low frequency tail are believed to be the four normal vibrational frequencies of SiO_4. The 1055 cm^{-1} band has been associated with a bond-stretching vibration in which the bridging oxygens move in opposite directions of the Si neighbors and roughly parallel to the Si-Si bond, while the 800 cm^{-1} band has been ascribed to a bond-bending type of motion in which the oxygens move approximately at right angle to the Si-Si bonds and in the O-Si-O planes[18]. Two sharp lines at 491 cm^{-1} and 604 cm^{-1} were suggested as due to modes localized around defect sites. The relative intensities of these lines were found to increase with neutron irradiation and decrease with the increasing dopant concentration of OH ions[5,6,17,19].

The broad peak at 1195 cm^{-1} is explained as the longitudinal optical (LO) mode of the transverse optical (TO) mode centered at 1055 cm^{-1}. Galeener and Lucovsky[15] have also treated the 490 cm^{-1} peak as the longitudinal optical mode of the transverse optical mode at 450 cm^{-1}.

Raman spectrum of vitreous SiO_2 is affected by defects. Water content, metalic impurties, intentionally introduced dopants and neutron irradiation play important roles in determining the properties of fused silica which could influence the optical transmission characteristics of fibers. It is well known that water content dominate the loss spectra of fibers in the spectral range between 1.2 to 1.8 μm, which can be a limiting factor in the transmission of optical fibers intended for long range optical communication systems. The most general model of water incorporation in vitreous silica is to assume that water is trapped at broken Si-O bond defects. The number of defects which depend on the fictive temperature (T_F) limits the amount of water content in glass[19]. Since water occupies the defect sites, one expects those defects to decrease with increasing OH content. This assumption could be proven by observing the relative intensities of 491 cm^{-1} and 604 cm^{-1} bands, which is believed to be caused by those defect centers, as a function of OH content. Indeed the relative intensity of these two lines decrease with increasing OH content, which is in agreement with the above model.

Effects of Cladding:

Fig. 2 also shows two very sharp peaks located at 2909 cm^{-1} and 2971 cm^{-1} which correspond to the two most intense lines of the polymer material[2]. From the occurence of these two peaks associated with

a plastic material, it could be concluded that the light actually propagates in the evanescent region of the cladding.

O'Connor and Tauc[2,3] has calculated the ratio of the coupling efficiency of light scattered in the cladding and in the core from the ratio of the relative intensity of these two new lines and that from the core material. The ratio of the relative intensities of the Raman lines from the cladding ($I_{R_{cl}}$) and the core (I_{R_c}) can be expressed as follows.

$$I_{R_{cl}}/I_{R_c} = (R_{cl}/R_c) \ (\sigma_{cl}/\sigma_c) \ (P_{cl}/P_1) \qquad (1)$$

where R_{cl} and R_c represent coulping efficiency into guided modes of light scattered in the cladding and core respectively; σ_{cl} and σ_c are the Raman cross-sections in the cladding and in the core; P_{cl} is the power of the exciting beam in the cladding; P_1 is the total power carried by the fiber.

The ratio of P_{cl} and P_1 has been derived by O'Connor and Tauc as

$$P_{cl}/P_1 = \frac{4}{3} \ N^{-\frac{1}{2}}$$

where N is the number of guided modes supported by the fiber and is given by $N = \frac{1}{2} \ v_o^2$ where $v_o = (\frac{\pi \ d}{\lambda})$ (N.A); d is the core diameter, λ is the wavelength of the exciting light, N.A. is the numerical aperature of the fiber. In our fiber with d = 0.25mm, n_{core} = 1.458, N.A. = 0.24 at steady state and excited at wavelength λ = 4880A°, we have N ≈ 74523. The relative cross-section of the 2909 cm^{-1} line of the plastic and the 1623 cm^{-1} line of the bulk samples of SiO_2 have been measured by O'Connor and Tauc and found $\sigma_{2909}/\sigma_{1623}$ ≈ 1.07 x 10^3.
We measured the ratio of the relative intensities of the 2909 cm^{-1} line

from cladding and 1623 cm^{-1} line from core and have $I_{2909}/I_{1623} \simeq 0.245$.
Using these values in equation (1) we obtain $R_{cl}/R_c \simeq 0.062$.
Theoretical values of R_c and R_{cl} have also been derived by O'Connor
and Tauc as follows:

$$R_c = \tfrac{1}{2}\ (N.A./n_{core}) \tag{2}$$

and

$$R_{cl} = \frac{3}{16}\ (N.A.)^2\ \frac{N^{-\tfrac{3}{2}}}{(1 + 1/(2N)^{\tfrac{1}{2}})}\quad \int_0^N \frac{2v\ dv}{\frac{\alpha d}{2} + 2(2N-2v)^{\tfrac{1}{2}}} \tag{3}$$

Because of the difficulty in evaluating the right hand side of the
equation (3) we estimate the R_{cl} values from its maxima and minima
which can be easily found by replacing the denominator in the
integrand by its minimum and maximum values. Thus, the range of R_{cl}
can be approximated by:

$$0.0524\ (N.A.)^2\ (1 + (2N)^{-\tfrac{1}{2}})^{-1} < R_{cl} < \tfrac{1}{4}\ (N.A.)^2\ \{1 + (2N)^{-\tfrac{1}{2}}\}^{-1}$$

From the above discussion, we estimate $R_{cl} \simeq 0.68 \times 10^{-2}$ and from
equation (2) we have $R_c = 0.013548$ and $R_{cl}/R_c \simeq 0.503$ which is much
larger than the experimental data $R_{cl}/R_c \simeq 0.062$. The discrepancy
is assumed to be due to imprefections or impurities that exist at the
core-cladding interface. It is thus possible that the quality of contact
between the core and the plastic cladding of optical fibers could be
determined from measuring their Raman spectra.

Doped Fibers:

Germania and B_2O_3 dopants also reduce the intensities of 491 and 604
cm^{-1} lines which indicate that these impurities also are located at the
defect sites [6,19]. Alkali impurities, however, do not cause a
reduction of 491 cm^{-1} and 604 cm^{-1} lines indicating that the alkali

oxides help breaking the Si-O bonds rather than being trapped at the defect sites. Fig. 3. shows the Raman spectrum in the frequency range from 3440 cm^{-1} to 3920 cm^{-1} illustrating a rather strong peak centered at 3690 cm^{-1} which is believed to be due to OH stretching mode. The relative intensity of this band, as expected, increases almost linearly with OH concentration. These measurements could therefore be developed into a conventional and reliable means of measuring water content in v-SiO$_2$[20] (and also in many other glasses). Fig. 4. is the amplified version for the frequency range of 800 cm^{-1} to 1200 cm^{-1} of the Raman spectrum of the high OH content PCS fiber which is shown in Fig. 1. This spectrum (Fig. 4) used higher excitation intensity and better resolution. A very weak peak located at 970 cm^{-1} which is due to Si-OH stretching mode, as expected, is much weaker than that of 3690 cm^{-1} OH stretching mode. The intensity of this band as estimated by Stolen and Walrafen[19] for wet SiO$_2$ (1400 PPM) to be about 7.5% of the 1200 cm^{-1} band. This band (3690 cm^{-1}) is usually hard to find in bulk samples[4] and is found to disappear in water free or low OH content SiO$_2$ core fibers. The intensity of this band also increases with increasing OH concentration. Si-O stretching mode frequency is located around 1100 cm^{-1}. This band has been observed by Stolen and Walrafen[19] in neutron irradiated samples. The dangling oxygen bonding, increased after irradiation, causes a filling in the minimum between 1065 cm^{-1} and 1200 cm^{-1} bands (because of an increase in the 100 cm^{-1} band intensity) and this minimum in wet silica seems deeper than in dry silica, due to a reduction of the number of dangling oxygen bonds as the defects

are filled with OH groups. Because of the strong fluorescence background for irradiated silica and very weak intensity of this (1100 cm^{-1}) band this effect is still difficult to be confirmed (measurement of the related anti-Stokes band can rule out the fluorescence effect but is too difficult to be observed because of low intensity). The 1100 cm^{-1} Si-0 stretching mode can be assigned by comparing the Raman spectrum of a slightly K_2O doped fiber and a pure SiO_2 core fiber. It is suggested that the K_2O impurities enter the SiO_2 structure by breaking Si-0 bonds rather than being trapped at existing defects. The 1100 cm^{-1} band which is caused by Si-0 stretching, can be estimated by calculating K_2O concentration and show good correspondence with experimental data[19].

A band due to Si-H stretching mode could not be found even in high OH content SiO_2 samples, but as reported by Hartwig[21], a Si-H stretching frequency at 2280 cm^{-1} had been observed in samples by dissolving hydrogen into the silica prior to irradiation (impregnated irradiated silica). This could be explained by the following reaction:

$$Si-0-Si + H_2 + radiation \rightarrow SiH + SiOH.$$
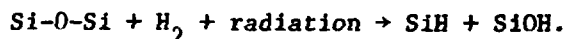
But in our "as - received" silica, water has been trapped in broken bonds forming two SiOH bonds:

$$Si-0-Si + H_2O \rightarrow 2SiOH$$
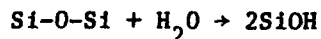
Thus no band due to SiH stretching mode could be observed. The SiH band is also reported by Van der Steen and Van der Boom in some kind of silica which contained hydrogen, and examined by using D_2 instead of H_2 to get the desired frequency shift[22].

Irradiation Effects:

Neutron irradiation of $v - SiO_2$ increases disorder by increasing the number of defects in the SiO_2 network, thus, causing some changes in the Raman spectrum. It has been reported[17,19] that in $v-SiO_2$ containing defects, the 491 cm^{-1} and 604 cm^{-1} bands may be due to modes localized about defect sites. The relative intensity of these two lines increases when the number of defects increases after irradiation. The nearest Si-Si distance decreases slightly in the irradiated material[17], thus resulting in an increase of bulk density of the sample and thereby causing the low frequency bands at 57, 450, 491 and 604 cm^{-1} slightly shift to higher frequencies. The continuum region of the main peak at 460 cm^{-1} (centered at 450 cm^{-1} for non-irradiated samples) is reduced, thus, decreasing the band width. This is explained as a transition from phonon—like states of the SiO_2 network (unirradiated) to more localized vibrational modes of many small regions of the heavily irradiated materials. Irradiation increases the defects and should increase the intensity of Si-0 (non-bridge oxygen) stretching mode at 1100 cm^{-1}. Because of the strong fluorescence after irradiation and relatively weak intensity of the band, this effect still can not be confirmed.

Second Order Spectrum:

Second order Raman spectrum of SiO_2 core fiber is illustrated in Fig. 2. The frequency range of 1400 cm^{-1} to 2600 cm^{-1} are considered as second order Raman spectrum of $v - SiO_2$ which are caused by the overtones of the first order mode frequencies or their combinations. From the spectrum it is clear that Raman peaks at 1610 cm^{-1}, 2130 cm^{-1}

and 2390 cm^{-1} are roughly twice the frequency of the first order lines at 800 cm^{-1} 1055 cm^{-1} and 1195 cm^{-1}. The peaks centered at 2028 cm^{-1} and 2247 cm^{-1} seem due to combination of first order lines of 1195 cm^{-1} and 800 cm^{-1}, and 1055 cm^{-1} and 1195 cm^{-1}, respectively.

Results on doped fused silica:

The fiber sample we used for doped-fused silica was a Galileo 30 m, 55 μm core, step index fiber with GeO_2 and P_2O_5 doping, low OH content and with numerical aperture of 0.25. The resultant Raman spectrum is shown in Fig. 5(a) and 5(b). Comparing the spectrum with those from the GeO_2 and GeO_2-B_2O_3 doped fused silica core fiber reported previously[5,6], we find that the spectra of the doped materials are not the superposition of the Raman spectra of the components. The effect of dopants on Raman spectrum of fused silica are two fold. Firstly, it produces new bands, like the ones located at 680 cm^{-1}, 930 cm^{-1}, 1034 cm^{-1} and 1360 cm^{-1} which do not appear in SiO_2 or the dopants. Secondly, the original peaks vary either in shpae, relative intensity or a small shifts in frequency. First we will discuss the SiO_2-GeO_2 system, then compare it with the SiO_2-GeO_2-P_2O_5 and SiO_2-GeO_2-B_2O_3 systems. The structure of vitreous SiO_2-GeO_2 system is generally regarded as a continuous network of nearly perfect SiO_4 and GeO_4 tetrahedras connected to each other. These tetrahadra are of similar size, thus, allowing the glass formation in a wide range of composition in the system GeO_2-SiO_2[24]. Silica doped with certain materials have reduced attenuation, and the refractive index increases with GeO_2 content. Thus GeO_2-SiO_2 core with pure SiO_2 cladding could be a good structure for optical fibers.

A look at the Raman spectrum of germania doped (about 10 ~ 15%)

40

fused silica core fiber reported by Walrafen and Stone[6], reveals that there are no typical bands of pure GeO_2. Germania bands only occur at very high concentration of germania doped fused silica[24,25]. We can assume that doped fused silica at this doping concentration do not contain GeO_2 as an individual phase. Comparing the Raman spectrum of pure SiO_2 and GeO_2-SiO_2 core fiber it is seen that the 450 cm^{-1}, 800 cm^{-1}, 1055 cm^{-1} and 1195 cm^{-1} peaks which arise from the silica network almost remain at the same position or slightly shift to lower frequencies. The amount of frequency shifts and the variation of relative intensities depend on germania concentration. This is because the tetrahedra structure of SiO_4 and GeO_4 of the vitreous silica and vitreous germania have almost the same size, and doping of Ge just substitutes some Si atoms with Ge atoms in the SiO_4 network. This Ge center SiO_4 network was suggested to mean that the Ge atoms do not break the Si-O bond but rather are trapped by already existing broken Si-O bonds. The basic structure of vitreous silica does not change too much, and because the Ge atom is heavier than Si atom the peaks caused by SiO_4 vibration still exist and results in some peak shift to lower frequencies. The 490 cm^{-1} and 604 cm^{-1} peaks were believed to be caused by the local mode of Si and -O-Si- defects centers in the silica network. Germania dopants are suggested to be trapped by these defects. Decreasing the concentration of these defects, the relative intensities of these two lines decreased; and because of the change of the structure, these two lines shift to 475 cm^{-1} and 575 cm^{-1}. A prominent band at 680 cm^{-1} and weak bands at around 1000 cm^{-1} to 1030 cm^{-1} which are caused by pure v-SiO_2 or v-GeO_2 are suggested to

41

be caused by the mixed Si-O-Ge bond. The band at 1000 cm^{-1} to 1030 cm^{-1} is intermediate between the frequency of the antisymmetric stretching vibration Si-O (1100 cm^{-1}) and Ge-O (890 cm^{-1}). The 680 cm^{-1} band is intermediate between the frequency of the symmetric stretching vibration Si-O (800 cm^{-1}) and Ge-O (570 cm^{-1}). These two bands have been shown appearing, growing and eventually disappearing from the infrared spectrum with increasing Ge concentration. This behavior is reminescent of one mode type behavior of a mixed crystal system[26].

Comparing Figs. 5(a) and 5(b) for GeO_2-P_2O_5-doped fused silica with the spectra of GeO_2-B_2O_3 and GeO_2-doped fused silica core fiber it is clear that all of them have almost the same peak positions as compared to only Ge-doped fused silica except for two new bands at 930 cm^{-1} and 1360 cm^{-1}. The 930 cm^{-1} band had been ascribed as Ti-O motion[18] in observation of Raman spectrum of T glass and has been ascribed as caused by B_2O_3 doping. But since this band is common in P,B,Ti doping, which have quite different atomic masses it is probable that the previous assignment of the 930 cm^{-1} band is incorrect. Kato[18] suggested that the 930 cm^{-1} band is caused by the dopant induced non-bridging oxygens, and explained that there is no 930 cm^{-1} band in the Al_2O_3-doped and GeO_2 doped fused silica, because Al_2O_3 and GeO_2 are very tight glass network formers. This assumption could be supported by infrared reflection spectra of neutron damaged silica including dangling oxygen bonds[19,27]. Kato also developed a method for the quantitative analysis of an additive in silica glasses with good results. But the 930 cm^{-1} band has not been found in fused silica even after neutron irradiation or doping with K_2O, which should increase

dangling oxygens. The 1350 cm^{-1} band was also found in the Raman spectra of all $GeO_2-P_2O_5$ doped and B_2O_3 doped fused silica, and was not found in the spectrum of GeO_2 doped fused silica. Even if the formation of 930 cm^{-1} and 1350 cm^{-1} bands is still not clear, one can be certain that these two bands are caused by dopants, and that the intensity is related to the doping concentration. It is thus suggested that these bands be used to estimate the concentration of dopants. However, the dopant concentration in fiber is not uniform across the core. Estimate of the dopant concentration depend on the actual propagation path of the light in the core, i.e. of the modal excitation of the fibers by the input light and thus relating to the launching condition.

It is known that the materials with more order have small Rayleigh wing and Raman peak band width. Thus it is of interest to compare spectra of quartz and glasses. Since Rayleigh scattering is an important limitation in optical transmission we are also interested in comparing the Raman peak band width in doped-fused silica and pure fused silica, which relate to the local order of material. From Figs. 1 and 5 , it is seen that, the most intense band at 450 cm^{-1} in pure and doped silica have half widths of 185 cm^{-1} and 125 cm^{-1}, respectively. It seems therefore that doped fused silica show a significant narrowing of the Raman bandwidth, which means it has more local order, and has less loss. It is in agreement with the fact that doped fused silica decreases the attenuation.

The Raman spectrum in the frequency region 1400 cm^{-1} to 3200 cm^{-1} of $GeO_2-P_2O_5$ doped fused silica core fiber is due to second order

43

processes, caused by either the overtone or the combination of the fundamental frequencies. With the aid of table II, it appears that the frequency shifts at 1592 cm^{-1}, 1856 cm^{-1}, 2060 cm^{-1}, 2297 cm^{-1} and 2765 cm^{-1} are the overtones of the first order frequencies at 800 cm^{-1}, 928 cm^{-1}, 1034 cm^{-1}, 1150 cm^{-1} and 1360 cm^{-1}. The frequency at 2146 cm^{-1} is due to the sum mode of 1034 cm^{-1} and 1150 cm^{-1}.

Low Frequency Raman Spectrum:

It has been found that the very low frequency Raman scattering from vitreous silica includes an excess scattered intensity, which varies almost linearly with temperature and can not be seen in the corresponding crystalline state. This is caused by the anomalous thermal properties of glasses and indicate that in addition to the acoustic phonons with a Debye distribution, some other phonon states may be present[28]. Until now, the identity of these additional states were unclear. In this section, we shall briefly review some theoetrical models that have been put forward to explain this excess scattered light[28-32]. As mentioned earlier, distinction is made between models based on Debye continuum model and others which we call the light-scattering excess (LSE) models. The continuum model proposed by Martin and Brenig (MB) is based on the disorder induced light scattering from acoustic phonons contributing to the low-frequency Raman scattering. The loss of translational symmetry leads to a breakdown of the wave vector selection rule and thus contribution from, more or less, all normal modes to the Raman scattering from an amorphous solid become possible. The vibrational modes in the low-frequency region are acoustic, thus, the density of states should be

Debye-like, and have a ω^2 dependency. The low-frequency Stokes scattering intensity could then be written as (see ref. 29):

$$I_{is}^{MB}(\omega) = \omega(n(\omega) + 1) \frac{\sigma^2}{v_1^2} \omega^2$$

$$\times (E_{is,si}^{1} \exp(\frac{\omega^2 \sigma^2}{v_1^2}) + (\frac{v_1}{v_t})^5 E_{is,si}^{t} \exp(\frac{\omega^2 \sigma^2}{v_t^2}))$$

where $n(\omega) + 1$ is the usual Bose-Einstein population factor. The prefactor $\omega(n(\omega) + 1)$ is approximately constant for small frequency shifts. The subscripts i and s identify the direction of polarization of the incident and scattered light, respectively. is = VV selects the polarized, and is = VH the depolarized spectra. v_1 and v_t are the sound velocities for longitudinal and transverse waves, respectively. 2σ is an average correlation length of the spatial fluctuations.

For low frequency ($\omega < 50$ cm^{-1}), one can neglect the exponential term and the coupling constant is like ω^2 as reported by Nemanich[30] and Lannin[33]. Then, the Stokes intensity can be simplified as:

$$I_{is}^{MB}(\omega) = \omega(n(\omega) + 1) \mathcal{J}_{is}^{MB} \omega^2. \tag{4}$$

The $\omega(n(\omega) + 1)$ term is approximately constant for small frequency shifts. Thus, the intensity of the Stokes peak has a ω^2 dependence at low frequencies. The MB model had been shown experimentally to represent the behavior of chalcogenide glasses[30] at very low frequencies. For experiments at higher temperatures, as $\omega \to 0$, the intensity of the scattered light is not zero and causes a central peak which can not be explained by the MB model. This temperature dependent LSE has been explained independently by Winterling[28], and Theodorakopoulos and Jackle (TJ)[32]. Another

deficiency of the MB model is that it fails to describe the depolarization spectrum[30]. Both TJ model or the model proposed by Winterling are based on the existence of two-level defect states which are responsible for the linear temperature dependent term observed in the low-temperature specific heat of glasses. These defects can decay or be excited in two ways. The quantummechanical tunneling, involving resonant absorption or emission of a phonon, occurs at low temperatures. At high temperatures oscillator levels are filled and thermally activated jumping across the barrier cause the dominant decay mechanism. The Winterling model suggested that for the low frequency band ($\omega_o \tau << 1$) (where ω_o denotes the phonon frequency and τ denotes the characteristic relaxation time), the thermally activated decay produces a low-frequency tail in the spectral profile of acoustic phonons. When $\omega_o \tau >> 1$, this tail seperates off from the main line and appears as a central mode with a full width at half-height approximately equal to $2 \tau^{-1}$. Light can then couple to the central mode and cause the observed LSE. The TJ model assumes that the two state defects exhibit different electric polarizabilities. Hopping of the defects between the two defect states is thermally activated. The thermally activated transition rate is $\tau_o^{-1} e^{-V/T}$ where V is the height of the central potential barrier, which is assumed to be equal for all defects that contribute to the observed "central peak". Thus the Stokes intensity could be written as[29]

$$I_{is}^{TJ}(\omega) = \omega(n(\omega) + 1) \; I_{is}^{OTJ} \; \frac{\tau}{1 + \omega^2 \tau^2} . \tag{5}$$

46

Combination of equs. (4) and (5) result in:

$$I_{is}(\omega) = \omega(n(\omega) + 1)\ (J_{is}^{OMB}\ \omega^2 + I_{is}^{OTJ}\ \frac{\tau}{1 + \omega^2\ \tau^2}) \qquad (6)$$

This combined equation includes the disorder-induced background and the Lorentzian line centered at $\omega = 0$, and is shown in Fig. 6(a) for PCS fiber for the frequency range of $-60\ cm^{-1}$ to $60\ cm^{-1}$. Fig. 6(b) shows the variation of intensity at three different temperatures. At very low frequency since the intensity has a ω^2 dependence the contribution of equation (4) can be neglected compared to the contribution from equation (5). Thus, the natural logarithm of $I_{is}(\omega) \times \omega^{-1} \times (n(\omega, T) + 1)^{-1}$ is linear with reciprocal temperature, and this result is shown in Fig. 6(c) for the temperature range we have studied. It should be noted that the PCS fiber used here ceases to guide light waves at temperatures below $-40^{\circ}C$.

References

1. R. Olshansky, Corning Technical Report. N.Y., # L 2362 (Feb. 1980)

2. P. O'Connor and J. Tauc, Opt. Commun. 24,135 (1978).

3. P. O'Connor and J. Tauc, App. Optics 17,3226 (1978).

4. R.H. Stolen, 'Proceeding of the 3rd. International Conference on Light Scattering in Solids', edited by M. Balkanski, R.C.C. Leite and S.P.S. Porto., John Wiley and Sons (1975).

5. G.E. Walrafen, Appl. Spectrosc. 29,179 (1975).

6. G.E. Walrafen and J. Stone, Appl. Spectrosc. 29,337 (1975).

7. J. Auyeung and A. Yariv, IEEE J. Quantum Electronics, QE-14, 347 (1978).

8. R.K. Jain, C. Lin, R.H. Stolen, W. Pleibel, and P. Kaiser, Appl. Phys. Lett., 30,162 (1977).

9. C. Lin, R.H. Stolen, W.G. French, and T.G. Malone, Opt. Lett., 1,96 (1977).

10. C. Lin, R.H. Stolen and L.G. Cohen, Appl. Phys. Lett., 31,97 (1977).

11. R.H. Stolen, C. Lin, and R.K. Jain, Appl. Phys. Lett. 30,340 (1977).

12. R.A. Steinberg and T.G. Giallorenzi, Appl. Optics 15,2440 (1976).

13. R.H. Stolen, IEEE J. Quantum Electronics QE-15,1157 (1979).

14. R. Rao, A.J. Corey and S.S. Mitra in 'Fiber Optics' Edited by B. Bendow and S.S. Mitra, Plenum Press, N.Y. (1979).

15. F.L. Galeener and G. Lucovsky, Phys. Rev. Lett. 37,1474 (1976).

16. F.L. Galeener and G. Lucovsky, 'Proceeding of the 3rd.
    International Conference on light scattering in solids',
    edited by M. Balkanski, R.C.C. Leite and S.P.S. Porto.,
    John Wiley and Sons, N.Y. (1975).

17. J.B. Bates, R.W. Hendricks and L.B. Shaffer, J. Chem. Phys.,
    61,4163 (1974).

18. Daisuke Kato, J. Appl. Phys. 47,2050 (1976).

19. R.H. Stolen and G.E. Walrafen, J. Chem. Phys. 64,2623 (1976).

20. F.L. Galeener and R.H. Geils presented by F. Galeener at the
    Symposium on the Structure of Non-crystalline Materials,
    Cambridge, England, (Sept. 1976).

21. C.M. Hartwig, J. Chem. Phys. 66,227 (1977).

22. G.H.A.M. Van der Steen and H. Van der Boom, J. Non-Crystalline
    Solids 23,279 (1977).

23. H.D. Bale, R.E. Shepler and G.W. Gibbs, J. Appl. Phys. 41,241
    (1970).

24. V.A. Kolesova and E.S. Sher, Inorgenic Materials 9,909 (1973).

25. V.M. Kostina, L.A. Zhukova, A.J. Kuznetsov, B.Z. Shalumov and
    E.A. Ryabenko, Inorgenic Materials 14,244 (1978).

26. I.F. Chang and S.S. Mitra, Adv. in Phys. 20,359 (1971).

27. I. Simon, J. Am. Ceram. Soc. 40,150 (1967).

28. G. Winterling, Phys. Rev., 12,2432 (1975).

29. F. Harbach, Phys. Stat. Sol., 95,533 (1979).

30. R.J. Nemanich, Phys. Rev. 16,1655 (1977).

31. A.J. Martin and W. Brenig, Phys. Stat. Sol. B 64,163 (1974).

32. N. Theodorako pulos and J. Jackle, Phys. Rev. B 6,2637 (1976).

33. J.S. Lannin, Phys. Rev. B 15,3863 (1977).

TABLE I

Comparison of Raman peaks of pure SiO_2 core fiber and bulk sample of SiO_2

Assignment	SiO_2 core fiber (cm^{-1})	Bulk SiO_2 (cm^{-1})
SiO_4 vibration	450	455
Defects	491	495
Defects	604	604
SiO_4 vibration	800	800
Si-OH stretch	970	
SiO_4 vibration	1055	1065
SiO_4 vibration	1195	1200
2nd order frequency	1610	1620
2nd order frequency	2028	2025
2nd order frequency	2130	2170
2nd order frequency	2247	2300
2nd order frequency	2390	2430
plastic peak	2909	
plastic peak	2971	
OH stretch	3690	3700

TABLE II

Comparison of Raman peaks of pure SiO_2 core fiber and doped fibers

| Assignment	P_2O_5-G_eO_2-doped fused SiO_4 core fiber	relative peaks in pure SiO_2 core fiber
revised-SiO_4 vibration	445	450
defects (reduced)	475	491
defects (reduced)	575	604
SiO-G_e bond	680	none
revised SiO_4 network	800	800
New band See Page 18	930	none
Si-O-G_e bond	1000 to 1030	none
revised SiO_4 network	1034	1055
revised SiO_4 network	1115 to 1175	1195
New band See page 18	1360	none
2nd order Raman spectrum	1596	1610
2nd order Raman spectrum	1856	none
2nd order Raman spectrum	2060	2130
2nd order Raman spectrum	2146	2247
2nd order Raman spectrum	2300	2390
2nd order Raman spectrum	2765	none
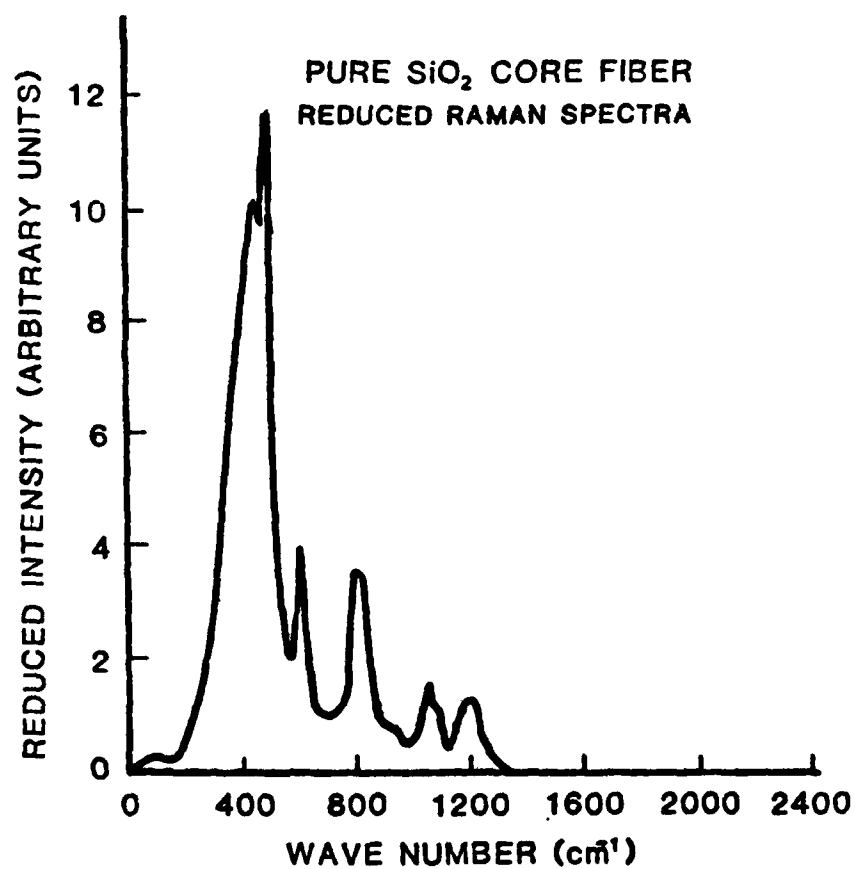
Figure 1. Raman spectrum of pure SiO_2 core fiber for $= 10 \text{ cm}^{-1}$ to 1300 cm^{-1}

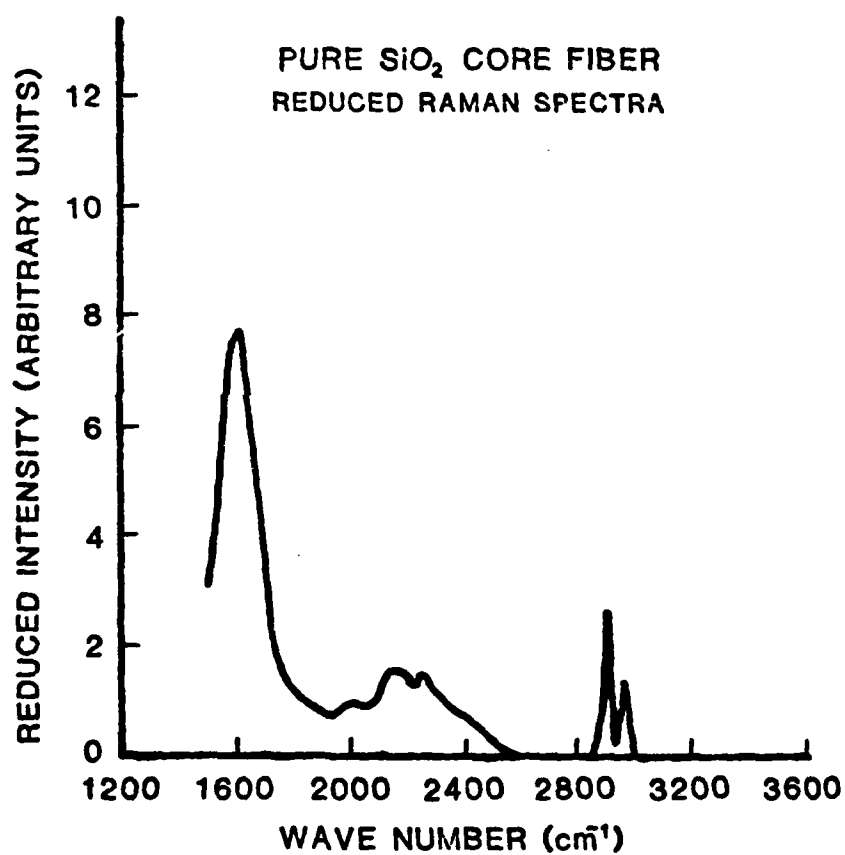Sample: Rank PCS-1 optical fiber

Excitation line: 6328A° (He-Ne laser)

Figure 2. Raman structure of pure SiO_2 core fiber for $\omega = 1300 \text{ cm}^{-1}$ to 3000 cm^{-1}.

Sample: Rank PCS-1 optical fiber
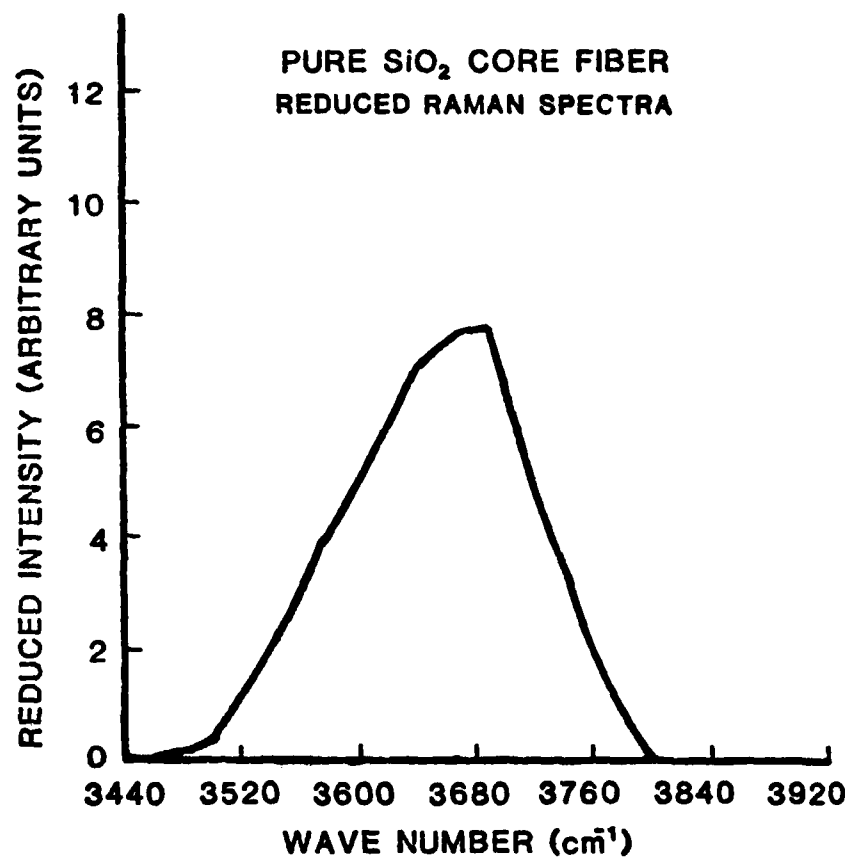
Excitation line: 4880A^o (Argon ion laser)

Figure 3.   OH stretching mode of high OH content pure SiO_2 core fiber
Sample: Rank PCS-1 optical fiber
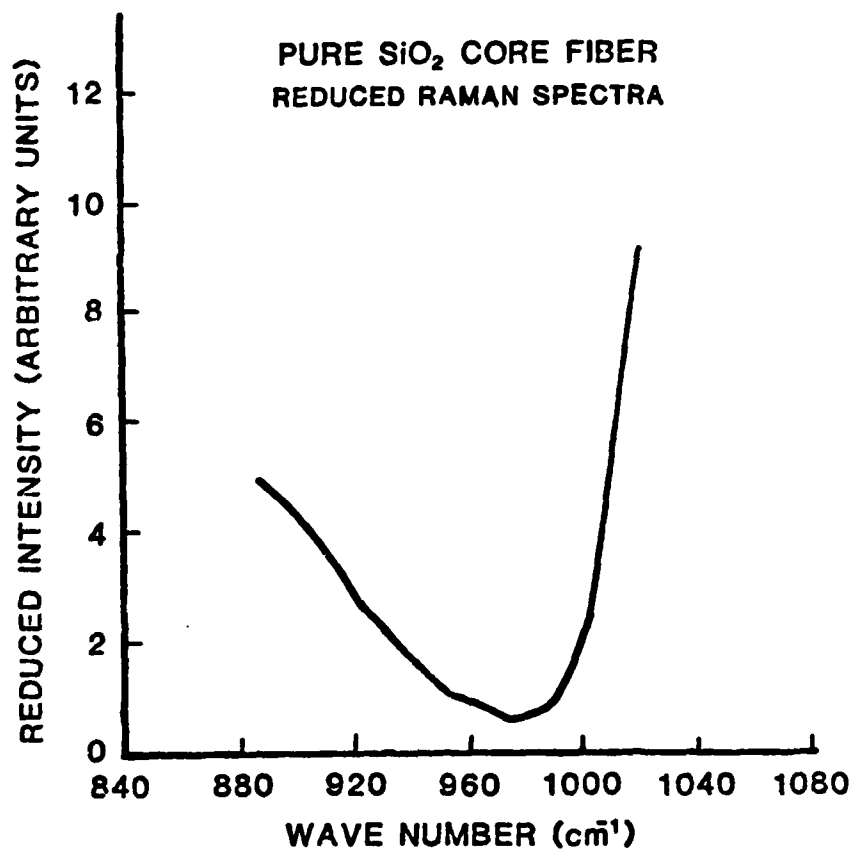Excitation line: 4880A° (Argon ion laser)

54

Figure 4. Si-OH stretching mode of high OH content pure SiO$_2$ core fiber
Sample: Rank PCS-1 optical fiber
Excitation line: 4880A$^\circ$ (Argon ion laser)

Figure 5(a). Raman spectrum of GeO_2-P_2O_5 doped fused silicon core fiber
for $\omega = 100$ cm^{-1} to $\omega = 1300$ cm^{-1}

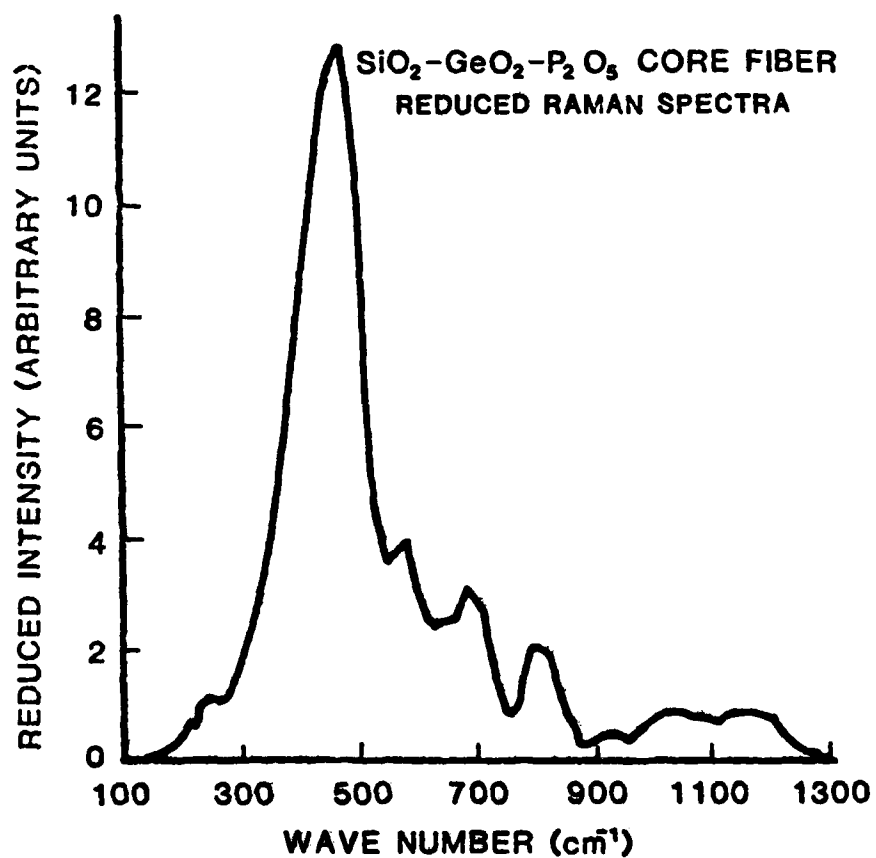Sample: Galileo optical fiber

Excitation line: 6328A^o (He-Ne laser)

56
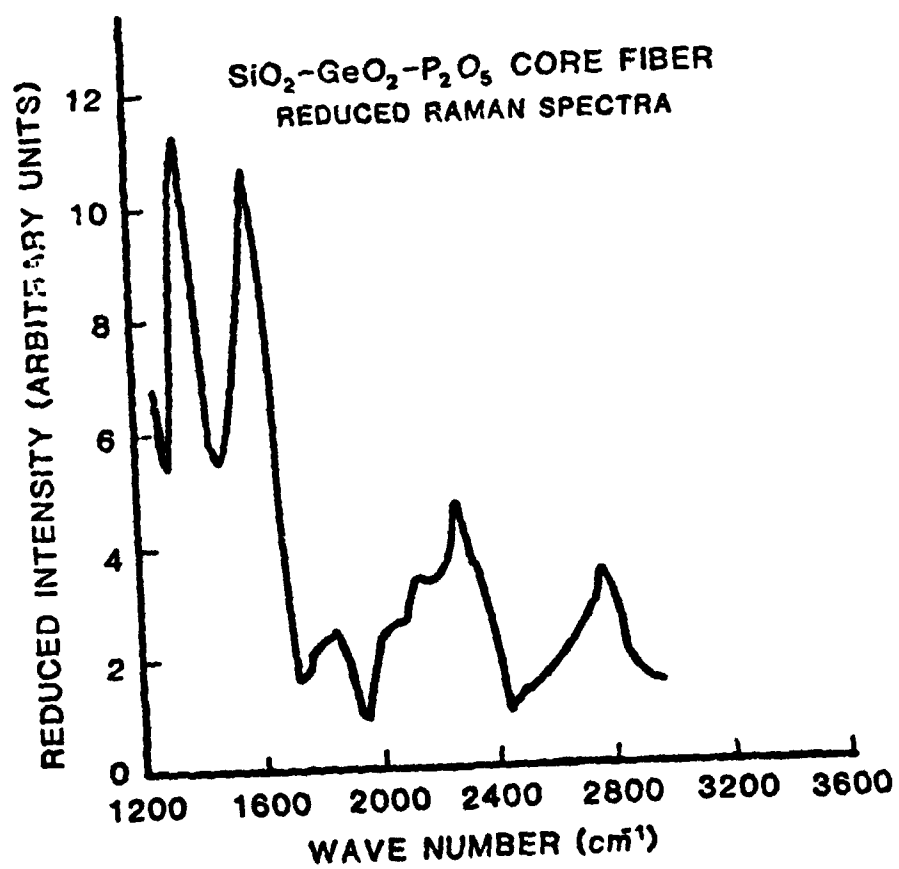
Figure 5(b). Raman spectrum of GeO_2-P_2O_5 doped fused silicon core fiber for $\omega = 1200$ cm^{-1} to $\omega = 3000$ cm^{-1}

Sample: Galileo optical fiber

Excitation line: 4880A$^{\circ}$ (Argon ion laser)

57
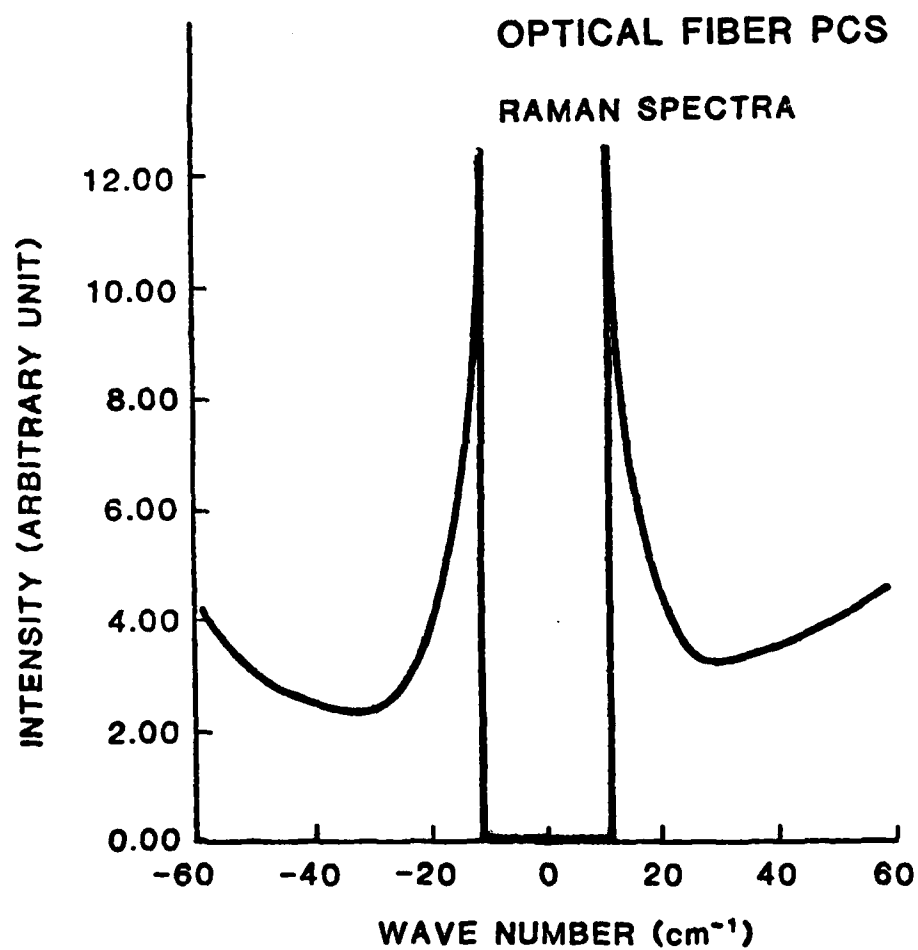
Figure 6(a). Low frequency Raman spectrum of optical fibers for $\omega = -60 \text{ cm}^{-1}$ to $\omega = 60 \text{ cm}^{-1}$

OPTICAL FIBER PCS
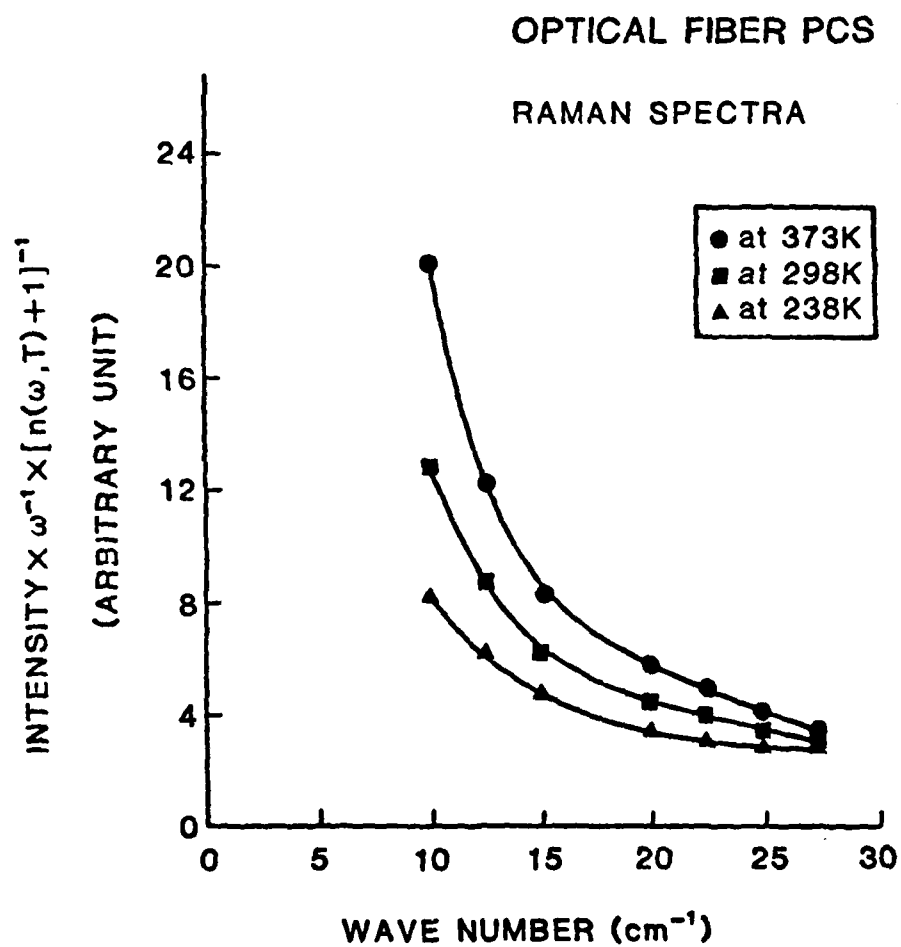
RAMAN SPECTRA

Figure 6(b). Low frequency Raman spectrum of optical fibers at different temperatures.

TEMPERATURE DEPENDENCE

$\omega = 10 cm^{-1}$ ●
$\omega = 12.5 cm^{-1}$ ▲
$\omega = 15 cm^{-1}$ ■

y-axis: $\ln[I_{is}(\omega) \times \omega^{-1} \times (n(\omega,T)+1)^{-1}]$

x-axis: $1/T \times 10^{-2}(K^{-1})$

Figure 6(c). Low frequency Raman spectrum of optical fibers showing the natural logarithm of the intensity as a function of reciprocal temperature.

60

APPENDIX I

ATTENUATION MEASUREMENTS

INTRODUCTION

The distribution of power between the various propagating modes in a fiber plays an important part in the measured attenuation levels[1]. Light injected at high launch angles can cause higher order modes to be excited which do not propagate through long distances. The loss per unit length near the input of the fiber is therefore generally greater than the loss per unit length further down the fiber, where a steady state distribution of power has been establ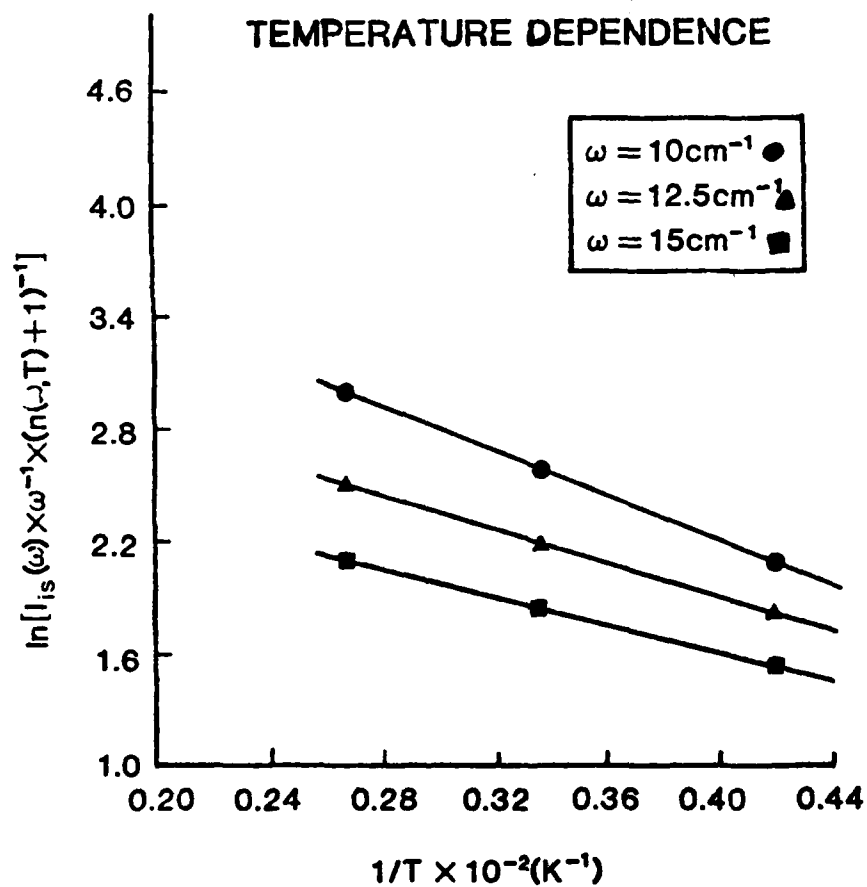ished. due to the loss of higher order modes and the process of mode conversion a steady state mode distribution usually does not occur within the first few hundred meters of fiber. Therefore, in normalizing attenuation to db/km a higher loss figure is obtained when short lengths of fibers are used to measure attenuation. Furthermore, other factors such as fiber spool diameter and winding tension can affect the attenuation due to excessive scattering.

Fiber attenuation can be computed from the power transmitted through two different lengths of fiber[2]. The power transmitted through a long length of fiber is measured. With the same input and output conditions the power transmitted through a short length of fiber is also measured. The loss per unit length can then be calculated. As mentioned earlier the results (loss per unit length) obtained can vary according to the fiber lengths being measured.

In this study, as the radiation induced change in the attenuation was of interest rather than the intrinsic fiber attenuation (as measured by the manufacturer), all the fibers could be fairly evaluated

and compared by using the same procedure and conditions in testing each fiber. Seventy meters of fiber was used in all cases but one. Of this 50 m was actually exposed to radiation in each case.

Figure 1 shows a schematic of the attenuation measurement set up. A monochrometer is used to filter the light from a tungsten light source. The monochrometer output is modulated by a mechanical chopper before injection into one end of the fiber. A silicon detector is butted up against the other end of the fiber. The detector output is connected to a lock-in amplifier in order to measure the amplitude of the received modulated signal. A detailed description of the equipment and procedures used to make the measurements is described below.

LIGHT SOURCE

A Bausch and Lomb high intensity monochrometer in conjunction with a tungsten light source was used. The spectral width of the monochrometer is adjustable and was set for a width of 50 nm.

OPTICAL CHOPPER

The monochrometer output was chopped by an AC synchronus motor turning a 13 blade chopper blade. a reference signal was generated by placing a detector and light bulb facing each other with the chopper blade in between. The output from the detector was coupled to the lock-in amplifier reference input.

INJECTION OPTICS

The chopped beam was roughly collimated and then focused through a microscope objective into the fiber. The N.A. of the microscope objective was chosen to be lower than that of the fiber so that as far as possible higher order modes were not launched and steady state conditions could be established in the relatively short lengths of fiber

that were used for the irradiations. A short length of fiber was stripped of jacketing material and painted black at the input end to prevent cladding modes from being launched. The fiber input end was positioned for optimum light injection by a 3-axis positioner.

DETECTOR

The output of the fiber was butted up against an EG SGD-100 detector. The detector was operated in the photoconductive mode at reverse bias of -30 volts and with a 1 μm load resistor. The detector was shielded from stray light by enclosing it with the fiber output end under a hood. This ensured that the detector was not driven into a nonlinear region by excessive stray illumination. The detector output was connected to the lock-in amplifier.

ELECTRONICS

The lock-in amplifier (PAR, HR-8) measured the amplitude of the transmitted signal. In some experiments, a chart recorder was connected to the lock-in amplifier to obtain a trace of the signal as function of time (Figures 7 & 8 in manuscript #II). In later experiments additional optics and a second lock-in amplifier was added to monitor the source intensity. A schematic of the latter setup is shown in Figure 2.
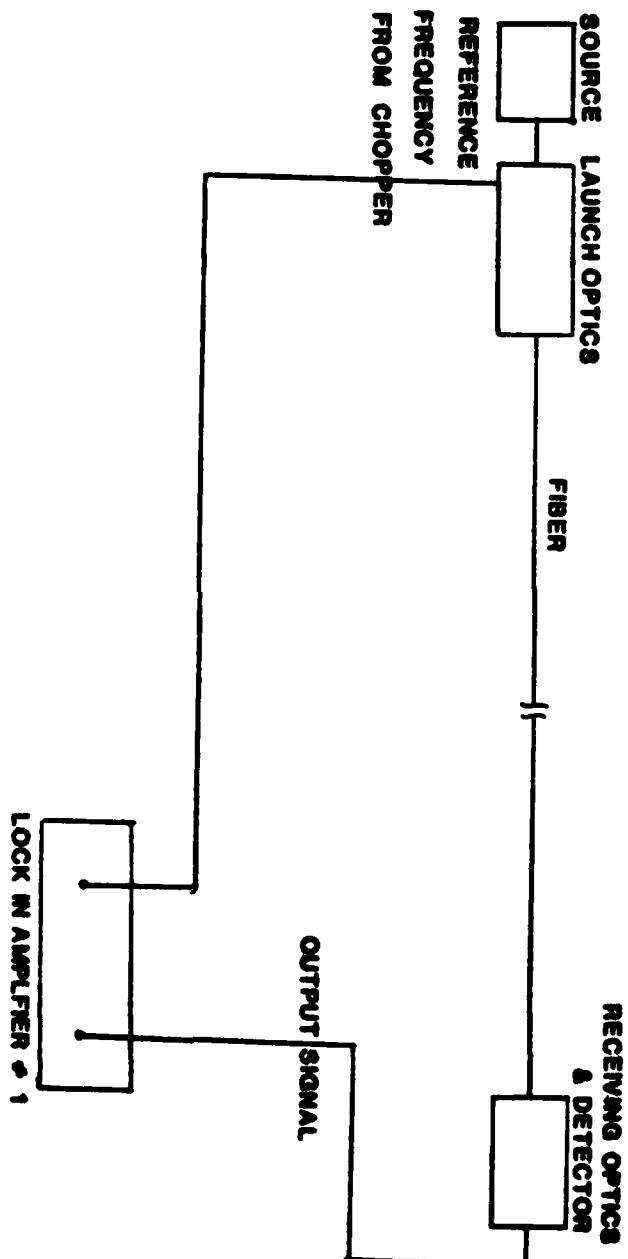
Figure 1. Schematic of attenuation measurement set up as used in earlier measurements.
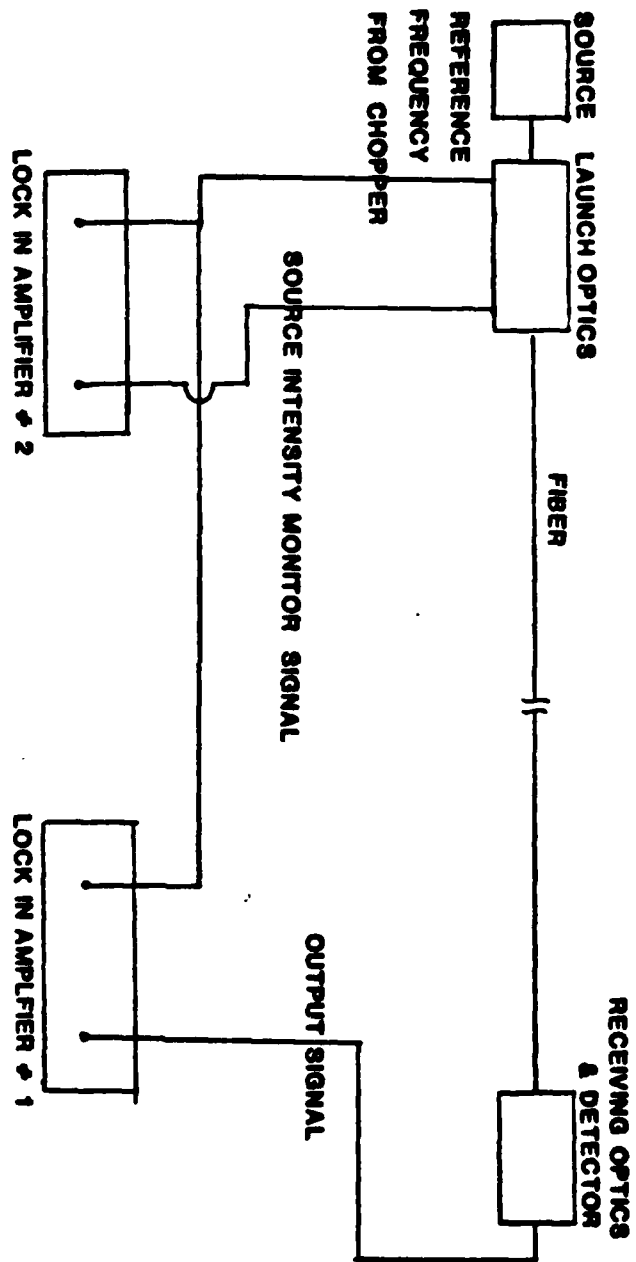
64

Figure 2. Schematic of attenuation measurement set up as
used in later experiments.

65

APPENDIX II

PULSE DISPERSION MEASUREMENTS

INTRODUCTION

Pulse dispersion in fibers is caused mainly by modal dispersion [3,4] and group velocity dispersion [5,6].

(i) Modal Dispersion: when narrow pulses are launched into a fiber causing all or a large number of modes to be excited the pulses spread out in time due to the different travel times of each mode. This is exemplified for a step index fiber in Figure 1.
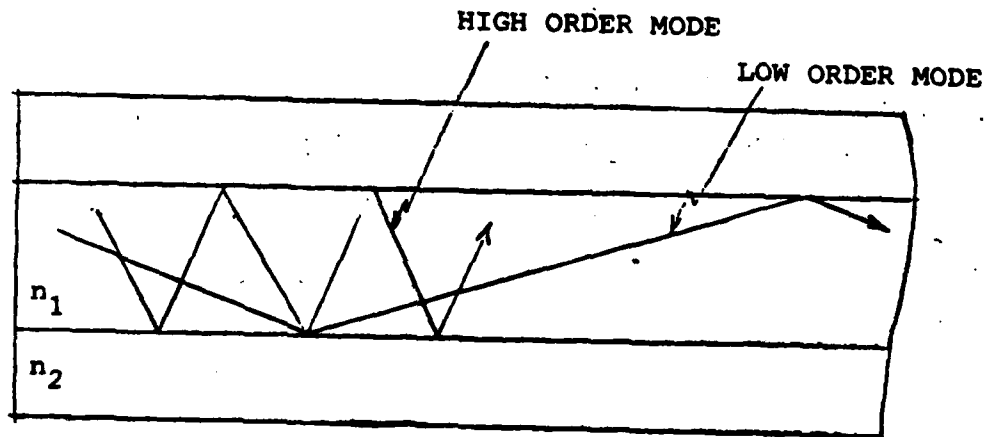
Figure 1. Ray paths in a step index fiber.

In a step index fiber rays travel zig-zag paths with the slowest ray traveling at the critical angle. The maximum delay between an axial ray and one traveling at the critical angle can be shown to be [7]

$$\Delta T = \frac{n_1 L}{c} \left(\frac{n_1 - n_2}{n_2} \right)$$

where L is the length of the fiber, n_1 is the refractive index of the core, n_2 is the refractive index of the cladding, and c is the speed

66

of light.

(ii) Group velocity dispersion: Since the index of refraction of glass is a function of wavelength, the speed of light in a fiber varies with wavelength. This causes pulses from a hroadband source to spread out in time by an amount proportional to the source bandwidth and fiber length. In multimode fibers, especially step index fibers, material dispersion is usually negligible in comparison to modal dispersion and the observed dispersion is almost exclusively due to modal dispersion.

Pulse distortion in ibers can be evauated by several different techniques [8-12]. In the time domain an impulse response measurement can be made to characterize the pulse broadening or in the frequency domain a frequency transfer function measurement can be made to characterize the bandwidth of the fiber. In order to measure pulse broadening a very short pulse must be injected into the fiber. This in effect causes all the modes to be excited instantaneously. At the output of the fiber the width of the broadened pulse is then an effective measure of the pulse broadening of the fiber. In the frequency domain approach, the short pulse corresponds to an impulse or excitation of all frequency components in the frequency domain. A Fourier transform of the output pulse then yields the bandwidth of the fiber.

In this study the pulse broadening technique is followed and pulse widths quoted are the FWHM widths of the pulses.

Figure 2 shows a schematic of the experimental set up that was developed to make pulse dispersion measurements. A very short optical pulse is generated by a laser diode. The pulse is injected into one end of the fiber. At the other end a high speed detector detects the output pulse. The detected pulse is displayed on a sampling oscillo-
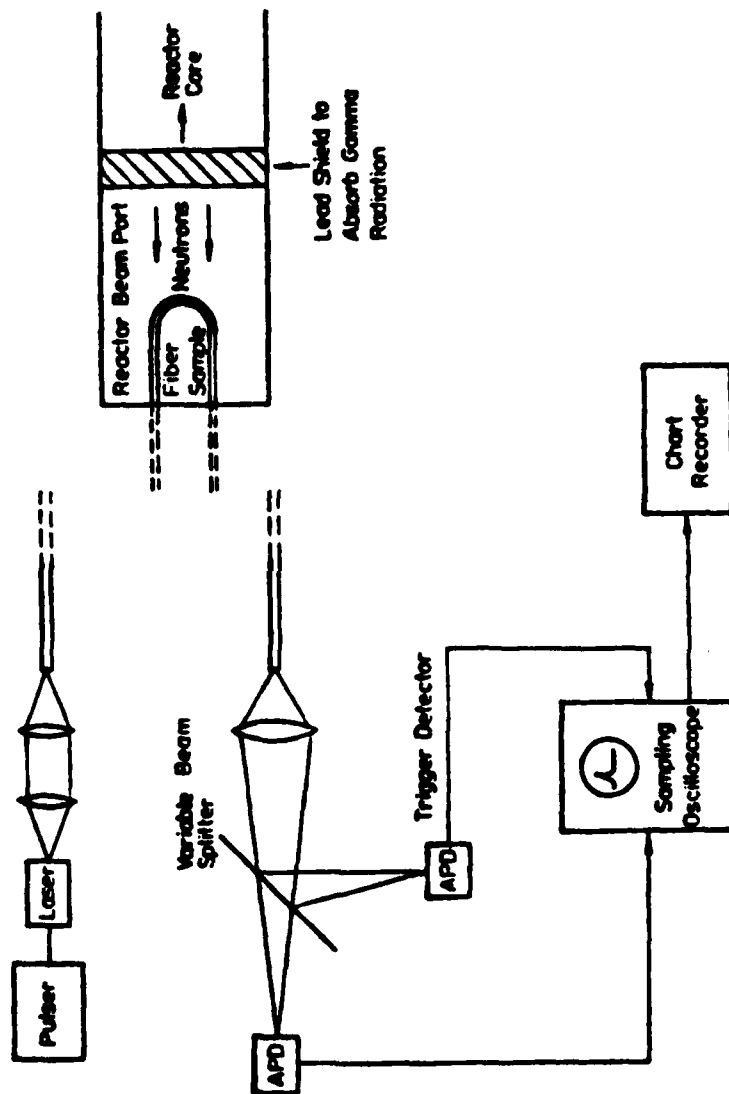
67

Figure 2. Experimental setup to measure change in pulse broadening as fibers are irradiated.

scope. A X-Y chart recorder is used to make a record of the pulse. A detailed description of the equipment and procedures used in making the dispersion measurements follows.
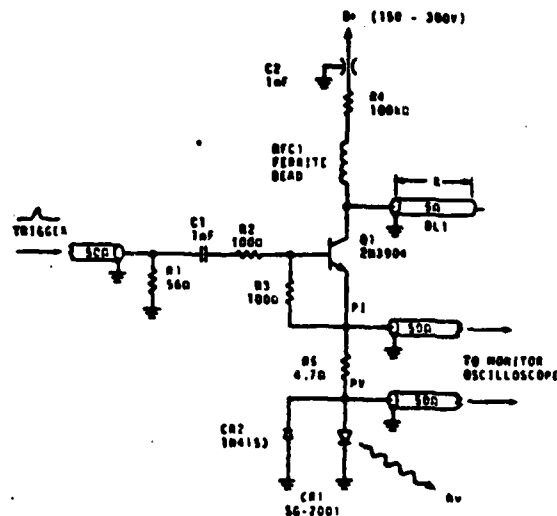
LASER DIODE

In order to measure pulse broadening a very short duration (1 ns) optical pulse is required. Furthermore, for experiments investigating radiation effects, the power launched into the fiber has to be adequate to compensate for both the intrinsic attenuation of the fiber and the expected radiation induced attenuation. Narrow high power optical pulses can be produced by GaAs lasers. The type chosen were Laser Diode Labs LD-60 single hetrostructure GaAs lasers. These lasers have threshold currents around 3 Amps for which a pulser was built. The chips are optically centered which make it easier to align with the injection optics. Experience has shown that not all such units are suitable for this application. Careful selection was required to select lasers with sharp enough rise and fall times and also with uniform field emission patterns. A number of lasers were purchased and usable devices were selected as described in the next section.

LASER DIODE PULSER

A drawback in the use of GaAs single hetrostructure lasers is the high currents required to pulse them. Typically threshold currents for this type of laser are around 3 amps and maximum allowable currents are around 10 amps. General purpose pulse generators are ot capable of delivering such high current short duration pulses. A transmission line pulse generator had to be assembled for this purpose from a design

69

by R.A. Andrews [11]. The circuit is shown in Figure 3.

Fig. 3. GaAs laser diode pulser circuit.

This pulser is capable of delivering 10 amp with a duration that can be adjusted by changing the length of the transmission line. A laser with the appropriate characteristics had to be selected before final assembly of the pulser. Some GaAs lasers are capable of producing a short pulse when the first of a series of Q switched spikes in their outputs can be excited [11], and provided this first spike is short. Starting with a test circuit and a long transmission line all the lasers were excited individually and a few were selected on the basis of a short first spike being present. The transmission line was then trimmed to a length such that only the first spike was excited. The output pattern of the selected lasers were examined by swinging a detector around its output face, a final selection was made of a laser

70

with the best overall characteristics. This resulted in a transmission line of 20 cms which corresponds to a pulse duration of 250 ps. The pulse generator circuit and laser were carefully mounted on a copper ground plane to eliminate noise problems as far as possible. A power supply (Power Designs Model 2K-10) was used to bias the circuit and an external pulse generator (HP-214) was used to trigger the circuit. The actual pulse width and amplitude could be varied somewhat by adjusting the bias voltage and trigger pulse amplitude. The maximum repetition rate of the pulse generator was restricted by the duty cycle of the avalanche transistor (2n3904) to 5 KHz.

DETECTOR

The RCA (C 20C92SE) detector was chosen for its high speed, high gain, and relatively low cost. The detector was operated in the photo-conductive mode with a 50 Ω load resistor and a reverse bias of 190 volts supplied by a Power Designs Model HV-1544 power supply. This resulted in a detector rise and fall time of 450 ps. The high gain of the detector eliminated the need for a wide band amplifier. The high speed measurement capability of the system was limited by the speed of the detector. Nevertheless the speed was adequate for the measurements being made.

OPTICS

The laser output was colliminated with a 20x, 0.40 N.A. (numerical aperture) microscope objective and launched into the fiber through a 10x 0.25 N.A. microscope objective. This results in the 75 μm x 2 μm emitting face of the laser to be imaged to a 150 μm x 4 μm spot on the

71

fiber face. The fiber was mounted on a 3-axis micropositioner which enabled the fiber face to be precisely positioned for maximum light injection into the fiber. With the microscope objectives properly aligned this point lies at the focal point of the second objective. The laser and pulser assembly, microscope objectives, and the 3-axis micropositioner were all assembled on a rigid platform so that alignment of the components once made would not be disturbed. The output end of the fiber was also mounted on a 3-axis positioner but as alignment was not critical at the detector end, coarse positioners were found adequate. A lens was required to focus the diverging fiber output into the small active area of the RCA detector. A variable beam splitter was positioned in between the lens and detector. This facilitated the adjustment of the beam intensity falling on the detector and also the excitation of a second detector. The output from the second detector could be used to provide a trigger to the oscilloscope that was used to observe the pulse.

ELECTRONICS

A high speed sampling oscilloscope system was used to observe the output pulse. This consisted of an HP-180c oscilloscope with a HP-1811a sampling plug in and a HP-1430c sampler. The oscilloscope system has a bandwidth of 18 Ghz. A trigger to the scope could be provided by either the pulse generator that was used to trigger the laser pulser or by the trigger detector. Each method had a drawback, but both methods were used in the set up procedure. A trigger pulse from the pulse generator had to be suitably delayed to compensate for the propagation time delay through the fiber. The drawback to this

method, however, was caused by timing variations in the delay between the trigger pulse to the laser pulser and the delayed pulse to the sampling scope. Due to the very short pulses being observed, small timing variations between the trigger pulse to the laser pulser and the delayed trigger to the scope caused excessive jitter making it very difficult to read pulse widths accurately.

This problem was eliminated by delaying the main or the first detector pulse through a long length of coaxial ($\approx$ 20m) cable and using the second detector's output to provide the trigger. The drawback to this method however was the slight broadening of the pulse that was caused by transmission of the pulse through the long length of the coaxial cable. The broadening, however, was negligible in comparison to the broadening through the long lengths (= 500m) of step index fibers that were being examined.

ALIGNMENT AND SET UP PROCEDURES

Alignment of the system was difficult due to the operating wavelength of the laser being in the infrared (904 nm). Particular difficulty was encountered at the source end in aligning the fiber with the focused laser beam. The technique devised to align the system is described next.

(1) A short length of fiber was used for the preliminary alignment. A HeNe laser beam was focused into the input end of the short fiber. The other end of the fiber was mounted on the triple axis positioner at the detector end. By adjusting the triple axis positioner the output from the fiber could be focused on the active area of the detector. The input end of the fiber was then mounted on the micropositioner at the

73

source end and the micropositioner adjusted to find the GaAs laser beam. Readjustment of the positioners at both ends of the fiber were made to maximize the signal received at the detector. A microscope was positioned at the input of the fiber with the fiber end in focus and oriented to lie in the cross hairs of the microscope. A fiber could therefore be aligned at the source quite accurately by adjusting the micropositioner to bring it into focus at the correct orientation against the cross hairs of the microscope tube. (The crude fiber mounts that were used did not allow a fiber to be mounted with repeatability at precisely the same position, and therefore some adjustment of the positioners was necessary every time a fiber was changed). With the preliminary alignment done the short length of fiber could be replaced with a longer length of fiber. The output end of the long length of fiber was positioned using the HeNe laser and the input end positioned by using the microscope. At this stage a signal was usually available at the detector but as final alignment had not been completed the signal strength was not always adequate to trigger the scope through the trigger detector. The delayed trigger from the pulse generator was set to correspond to the delay time through the fiber and was thus used initially to maximize the signal at the detector. Once the adjustments were made with the positioners to maximize the signal received the scope trigger could be provided by the trigger detector. With the pulse displayed on the sampling oscilloscope the X-Y chart recorder could be set to make a record of the pulse.

74

APPENDIX III

The Kramer-Kronig Relations

The refractive index of a material is given by

$$N(w) = n + ik$$

where n is the real part of the refractive index and k is the imaginary part or extinction coefficient. These two parameters are spectrally dependent and determine the optical behavior of a solid. An integral relationship exists between these two parameters which makes it possible to determine one of the optical constants provided the spectral dependence of the other constant is known. Specifically they are related by the Kramer-Kronig[14] relation as given by Cardona[15].

$$n(\omega) - 1 = \frac{2}{\pi} \, P \int_{o}^{\infty} \frac{\omega' k(\omega)}{(\omega' - \omega_r^2)} \, d\omega'$$

and

$$k(\omega) = \frac{2\omega_r}{\pi} \, P \int_{o}^{\infty} \frac{n\,(\omega)}{(\omega_r^2 - \omega'^2)} \, d\omega'$$

where P represents the Cauchy principal part

$$P \int_{-\infty}^{\infty} \frac{1}{\omega' - \omega_r} = 0$$

k is related to the absorption coefficient α of a material by

$$\alpha = \frac{4\pi k}{\lambda}$$

Because of the interdependence of n and k, it is obvious that one can-

not change without a change in the other.

This is an important consideration insofar as damage to optical materials by radiation is concerned. The increases of the absorption coefficient in irradiated glasses is due to change in k (or α) which must be accompanied by a change in n. In optical fibers, therefore, where radiation is observed to induce absorpton changes, changes in n must also result.

APPENDIX IV

PROPAGATION EFFECTS

The propagation effects in a fiber are determined by several factors such as its physical dimensions and the optical constants of the fiber materials. When irradiated, changes in the optical constants of the core and cladding materials can result. These changes may have varying influences on the many different propagating modes of a multi-mode fiber, resulting in changes in the power distribution, and the mode pattern. It is therefore necessary to consider the power flow of the guided modes when investigating radiation effects on the fiber. The power flow for the simplest case which is the step index multi-mode fiber is discussed. It is necessary to start with a brief review of how the various modes evolve.

A step index optical fiber consists of homogeneous cylindrical core surrounded by a cladding of lower refractive index as shown in Figure 1.
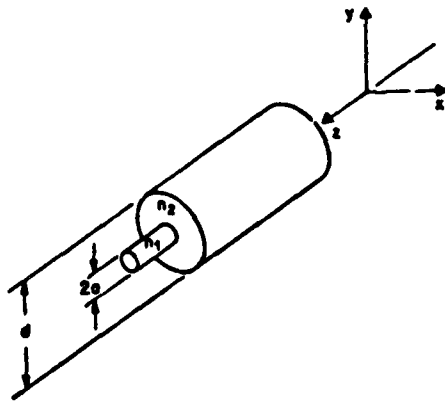

Fig. 1. Cladded optical fiber.

The waveguide core supports a finite number of guided modes which depend on the physical dimensions of the guide and the refractive indeces of the core and cladding materials. The electromagnetic fields propagating in the Z direction can be written as

$$\bar{E}\ (r,\ \theta,\ z,\ t) = \bar{E}(r,\theta)\ e^{i(\beta z - \omega t)}$$

$$\bar{H}\ (r,\ \theta,\ z,\ t) = \bar{H}(r,\theta)\ e^{i(\beta z - \omega t)}$$

where β is the propagation constant in the Z direction, ω is the angular frequency (r,θ) are the cylindrical coordinates and t is the time.] When β is real and such that

$$n_1 k \geq |\beta| \geq n_2 k$$

[where n_1 is the refractive index of the core and n_2 is the refractive index of the cladding and k is the propagation constant in free space,] a finite number of guided mode solutions exist. For this class of solutions, guided propagating fields exist in the core and can be described in terms of the Bessel function. The field in the cladding decays exponentially and can be described in terms of the modified Hankel function. The number of guided modes increases in terms of a parameter V defined as[16]

$$V = \frac{2\pi a}{\lambda}\ (n_1{}^2 - n_2{}^2)^{1/2}$$

[where a is the radius of the fiber core.] It is convenient at this

78

point to also introduce parameters U and W defined as

$$U = a(n_1^2 k^2 - \beta^2)^{1/2}$$

$$W = a(\beta^2 - n_2^2 k^2)^{1/2}$$

then

$$V = (U^2 + W^2)^{1/2}$$

In the weakly guiding approximation, the tangential field components of the electric and magnetic fields can be matched at the core cladding interface to yield the eigenvalue condition[16]

$$U \frac{J_{\ell+1}(U)}{J_\ell(U)} = W \frac{K_{\ell+1}(W)}{K_\ell(W)}$$

This is the characteristic equation for the linearly polarized modes (LP modes*). since J is an oscillatory function, a solution exists between each zero of $J_{\ell+1}$ (U) (the left hand side of the equation oscillates between $-\infty$ to $+\infty$). For each ℓ there are many solutions (the total number of which are limited by the v value of the fiber) each of which is a propagating mode. The modes are designated by the integer subscript ℓ,m where m gives the successive solutions to the boundary condition involving J_ℓ. The modes are, therefore, labeled LP_{01}, LP_{02}, LP_{11}, etc.

The power density of a mode in the core and cladding can be shown

---

*with $n_1 = n_2$, the $LP_{\ell m}$ modes break up into modes that are identified as $HE_{\ell-1,m}$ and $EH_{\ell-1,m}$ modes[2].

to be[16]

$$P_{core}(r,\theta) = K_{\ell} \frac{U^2}{V^2} \frac{2P}{\pi a^2} \frac{J_{\ell}^2(U\frac{r}{a})}{J_{\ell}^2(U)} \cos^2 (\ell,\theta)$$

$$P_{clad}(r,\theta) = K_{\ell} \frac{W^2}{V^2} \frac{2P}{\pi a^2} \frac{K_{\ell}^2(W\frac{r}{a})}{K_{\ell}^2(W)} \cos^2 (\ell,\theta)$$

where

$$K_{\ell} = \frac{K_{\ell}^2 (W)}{K_{\ell-1}(W) \, K_{\ell+1}(W)}$$

and P is the total power in the mode.

For large values of x $K(x)$ decays exponentially[3].

$$K_{\ell}(x) \to \sqrt{\frac{\pi}{2}} \quad e^{-x}$$

$$x \to \infty$$

Therefore, for large values of W the field is tightly bound to the waveguide and the field in the cladding decays rapidly. Close to the cut off, however, $W \to 0$ and the field ceases to be guided in the core and becomes a radiation mode. The total powers P in the core and cladding can be shown to be[16]

$$P_{core} = \left[1 + \frac{W^2}{U^2} \frac{1}{K} \right] \left(\frac{\pi a^2}{2}\right) \left(\frac{\mu_o \, \epsilon_o}{\mu_{core}}\right) \, E_{\ell}^2(a)$$

$$P_{clad} = \left[\frac{1}{K} - 1\right] \left(\frac{\pi a^2}{2}\right) \left(\frac{\mu_o \epsilon_o}{n_{clad}}\right) E_{\ell}^2(a)$$

where E is the electric field strength at the interface. From the power flow equations, it becomes obvious that the attenuation and phase velocities of each mode are determined by the optical constants of the core and cladding and the power distribution between them. A useful plot of the power fraction in the cladding vs. the waveguide V value is shown in Figure 2. As V increases, each mode becomes more strongly confined to the core.

Alternatively for a given V, the modes close to cut-off are shown to have a higher percentage of power in the cladding than the low order modes.

An approximate attenuation coefficient valid for $n_1 > n_2$ has been shown to be[17]

$$\alpha = \frac{\alpha_1 P_{core} + \alpha_2 P_{clad}}{P}$$

where α_1 and α_2 are the bulk obsorption coefficient of the core and the cladding materials.

The phase velocity v_p for a mode also varies according to the power distribution

$$\frac{c}{n_1} \leq v_p \leq \frac{c}{n_2}$$

Thus the phase velocity varies between the values it would have in the core or the cladding bulk materials. For low order modes, since the decay in the cladding is quite rapid v_p approaches $\frac{c}{n_1}$. Close to the cut-off, when the field is only loosely bound to the core, the phase velocity approaches $\frac{c}{n_2}$.

From this discussion, it is evident that when irradiated, all modes

of a fiber cannot be equally influenced. Low order modes with most power confined to the core are influenced predominantly by changes in the core materials. High order modes however, with a greater proportion (than low order modes) of power in the cladding, may be significantly influenced by effects of radiation on the cladding material.
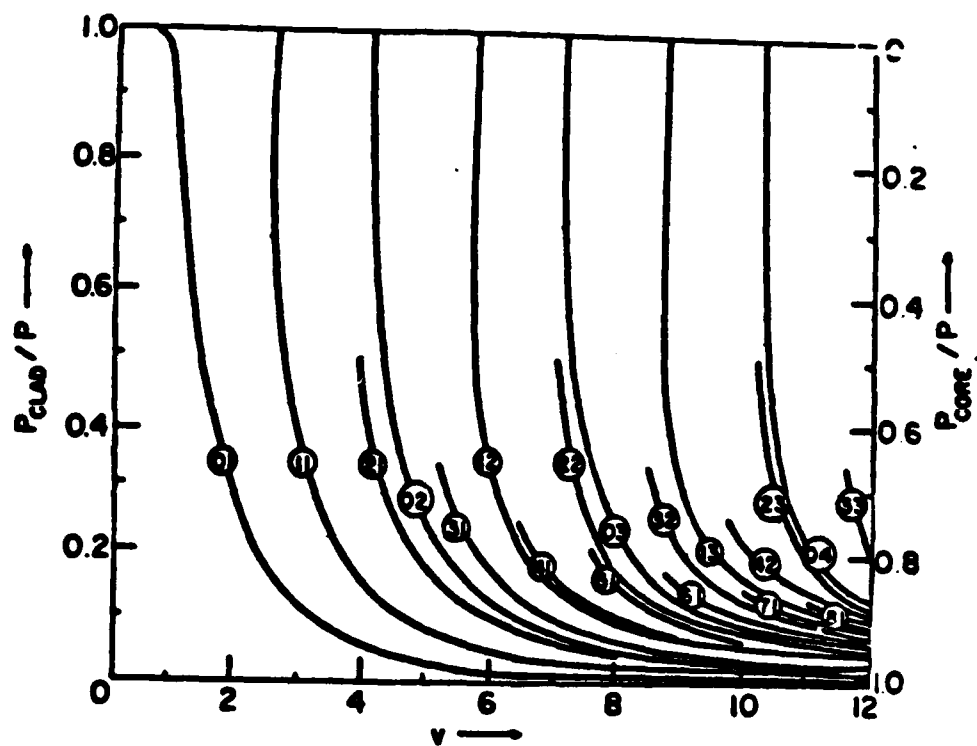
Figure 2. Ratio of mode power which propagates in the
cladding to the total power in the mode plotted
vs. V, the normalized frequency.

RADIATION EFFECTS

INTRODUCTION

The effect of radiation on matter is a vast subject by itself. In this Appendix, we will give a brief summary of effects of radiation on solids irradiated in a reactor, particularly glass and glass fibers.

Damage to solids is produced by numerous radiation sources including ionizing radiation (such as gamma rays) and particle radiation (such as neutrons).

Ionizing radiation generates free electrons or holes when interacting with matter. Thus ultraviolet light with energies of 10 eV, x-rays with energies of 10 to 100 k eV, gamma rays with energies of 1.25 MeV, and high energy electrons (100 k eV to 10 M eV) are examples of ionizing radiation. High energy protons (2 - 20 M eV), because of their large mass, are also an example of ionizing radiation. With the exception of x-rays these sources are not especially penetrating. Neutron radiation, however, is highly penetrating as neutrons are not charged and do not interact with the electric field around atomic nuclei. The damage therefore is not restricted to the surface region but is distributed throughout the solid.

REACTOR IRRADIATION

In reactor cores the ingredients of the fission flux include neutrons of varying energies, nuclei from fission fragments, x-rays and electrons. This includes both ionizing and particle radiation. The overwhelming majority of displacement events in reactor irradiated solids are initiated by primary events involving neutrons. The thermal neutrons with energies of 1/40 eV are in thermal equilibrium with the

84

environment and have insufficient energy to cause atomic displacements. The neutrons with energies greater than 2 k eV are referred to as fast neutrons and can cause atomic displacements. In the reactor fast neutrons with energies greater than 2 M eV are also produced.

DAMAGE TO MATTER

the defects produced by energetic particle irradiation depends on the nature and energy of the incident particle and also on the structure of the solid being irradiated. The incident particle shares its energy with the atoms in the solid which, as mentioned, can cause the atoms to be displaced or ejected from their lattice sites. This leaves behind a vacancy. The energy required to cause the displacement depends on the strength with which the atoms are bound to their sites. In glass, high energy particle bombardment may involve the displacement of ions in the glass lattice or substrate, resulting in changes in the glass density and absorption spectra. Secondary radiation from the particle irradiation can result also causing color centers. The damage center observed in pure fused silica is known to be in the silicon E' center. The E' center is an electron trapped on a silicon orbital which projects into an oxygen vacancy. The damage center in doped or impure glasses are to a great degree dependent on the doping or impurity content.

DAMAGE SOURCES IN GLASS FIBERS

In glass fibers dopants are introduced to alter the index of refraction of the silica. The introduction of dopants such as germanium not only increases the sensitivity to radiation but also results in the creation of different defect centers. ESR data, which has been

85

used successfully to study the damage in glasses, indicate that the damage in doped fibers is associated with charge trapping at the site of the impurities   Interpretations of ESR data and absorption spectra in fibers indicate electrons trapped at the site of an O_2 vacancy in an Sp^3 orbital of a germanium with one or two next nearest neighbors of germanium ions.

Efforts have also been made to reduce the efficiency of these charge trapping processes by adding metallic ions such as cerium. The results however have not been satisfactory because of the high intrinsic absorption losses introduced by the dopants. Furthermore the mechanism by which these dopants protect the fibers is not well understood. Efforts to heat treat the doped glass fibers in oxygen have been partially successful . Doped fibers appear to have oxygen vacancies that can be healed by heat treatment . However, the treatment of pure fused silica by heat has only been partially effective indicating the oxygen vacancy concentration to be low .

Limited success in protecting fibers from radiation leave fibers too sensitive for many applications. Pure fused silica still remains the least sensitive to radiation. However, mechanical problems associated with PCS fibers incorporating high purity silica cores warrant further work on protecting doped glass fibers.

Bibliography

1. R.D. Maurer, Proc. IEEE, 123, 591 (1976).

2. D.B. Keck and A.R. Tynes, appl. Opts. 11, 1502 (1972).

3. D.B. Keck, Appl. Opts. 13, 114 (1974).

4. S.D. Personik, Bell Syst. Tech. J., 50, 843 (1972).

5. R.B. Dyott and J.R. Stein, Electron. lett., 7, 82 (1972).

6. M. DiDomenico Jr., Appl. Opts., 11, 652 (1972).

7. Michael K. Barnoski, and S.D. Personick, Proc. IEEE, 66, 429 (1978).

8. Jurgen W. Dannwolf, Samuel Gottfried, G. Arthur Sargent and Robert C. Strum, IEEE Trans on Instrumentation and Measurement, 25, 404, (1976).

9. R.W. Dawson, Appl. Opts. 13, 264, (1974).

10. S.D. Personick, W.M. Hubbard, and W.S. Holden, Appl. Opts. 13, (1976).

11. L.G. Cohen, H.W. Astle and I.D. Kaminow, Bell Syst. Tech. J. 55, (1976).

12. Detlef Gloge, Arthur R. Tynes, Michael A. Duguay, IEEE J. of Quan. Elect., 8, 217 (1972).

13. J.R. Andrews, Rev. Sci. Instrum. 45, 22 (1976).

14. R. del. Kronig, J. Opt. Soc. Am. 12, 547 (1926); H.A. Kramers, AHi Congr. Intern Fis., Como 2, 545 (1927).

15. M. Cardona, in Optical Properties of Solids, ed. by S. Nudelman and S.S. Mitra, (Plenum, N.Y., 1969), pp. 137-157.

16. D. Gloge, Appl. Opt. 10, 2252 (1971).

17. N.S. Kapany, J.J. Birke and C.C. Shaw, J. Opt. Soc. Am., 53, 926 (1963).

MISSION
of
Rome Air Development Center

RADC plans and executes research, development, test and selected acquisition programs in support of Command, Control Communications and Intelligence (C^3I) activities. Technical and engineering support within areas of technical competence is provided to ESD Program Offices (POs) and other ESD elements. The principal technical mission areas are communications, electromagnetic guidance and control, surveillance of ground and aerospace objects, intelligence data collection and handling, information system technology, ionospheric propagation, solid state sciences, microwave physics and electronic reliability, maintainability and compatibility.